applied sciences

MDPI

Article

On the Use of FOPID Controllers for Maintenance Phase of General Anesthesia

Nicola Paolino [1], Michele Schiavo [1], Nicola Latronico [2,3], Fabrizio Padula [4], Massimiliano Paltenghi [3] and Antonio Visioli [1,*]

[1] Department of Mechanical and Industrial Engineering, University of Brescia, 25123 Brescia, Italy; nicola.paolino@unibs.it (N.P.); michele.schiavo@unibs.it (M.S.)
[2] Department of Medical and Surgical Specialties, Radiological Sciences and Public Health, University of Brescia, 25123 Brescia, Italy; nicola.latronico@unibs.it
[3] Spedali Civili of Brescia, 25123 Brescia, Italy; massimiliano.paltenghi@asst-spedalicivili.it
[4] Curtin Centre for Optimisation and Decision Science, Curtin University, Bentley, WA 6102, Australia; fabrizio.padula@curtin.edu.au
* Correspondence: antonio.visioli@unibs.it

Abstract: This paper investigates the performance achievable with a fractional-order PID regulator controlling the Depth of Hypnosis (measured via the Bispectral Index Scale) through the administration of propofol during the maintenance phase of total intravenous anesthesia. In particular, two different methodologies were applied to tune the controller: in the first case, genetic algorithms (GAs) were used to minimize the integrated absolute error, while in the second case, the isodamping approach—a method that targets phase margin invariance with respect to the process dc gain—was employed. In both cases, the performance was extensively analyzed and compared with that of a standard PID controller by simulating multiple patients through a Monte Carlo method. The results demonstrate that a fractional-order PID controller can be effectively used to control the Depth of Hypnosis, but the improvement with respect to a standard PID controller is marginal.

Keywords: anesthesia control; FOPID control; PID control; tuning

Citation: Paolino, N.; Schiavo, M.; Latronico, N.; Padula, F.; Paltenghi, M.; Visioli, A. On the Use of FOPID Controllers for Maintenance Phase of General Anesthesia. *Appl. Sci.* **2023**, *13*, 7381. https://doi.org/10.3390/app13137381

Academic Editor: Alessandro Gasparetto

Received: 16 May 2023
Revised: 15 June 2023
Accepted: 19 June 2023
Published: 21 June 2023

1. Introduction

Many closed-loop control algorithms for total intravenous anesthesia (TIVA) have been developed in the last several years [1,2] because of the benefits that an automatic control system can provide in this context. In fact, an effective control system can be a valuable tool for the anesthesiologist, who supervises the overall system, because it has the potential to limit errors caused by distraction and to reduce possible drug overdosing and underdosing, thereby increasing the safety of the patient.

Although in TIVA, analgesia and neuromuscular blockade should also be provided, the main task generally requires controlling the Depth of Hypnosis (DoH) through the hypnotic drug propofol. A feedback control system can be implemented by measuring the DoH by means of a processed electroencephalogram (pEEG) mechanism. Among these techniques, the most common one is the Bispectral Index Scale (BIS), which provides a measure of the DoH ranging from 100 (fully awake patient) to 0 (flat EEG). The overall anesthesia process consists of three phases. At the beginning, there is the induction phase, where the BIS has to be driven to the set-point value of 50 in a time interval of less than 5 min and without an excessive undershoot that might cause problems for the patient. Usually, this is achieved through the administration of a bolus of propofol, where the amount of drug depends on the physical characteristics of the patient (thus, a feedforward action is applied from a control system point of view). Once the BIS has settled to the set-point value, the maintenance phase starts. During maintenance, the control task is to keep the BIS in the range from 40 to 60 despite the surgical activity and the presence of noxious

stimuli (excessively low values can result in dangerous hypotension or burst suppression episodes, while excessively high values can result in traumatic patient awareness). Finally, in the emergence phase, drug administration is stopped, and the patient wakes up. The maintenance phase can last for hours and is critical in anesthesia, which implies that a control system should be designed by mainly considering the disturbance rejection task. Further, the controller should also be robust to intra- and inter-patient variability, since satisfactory clinical outcomes should be guaranteed for all patients.

The nonlinearity of the pharmacokinetic/pharmacodynamic (PK/PD) model [3] makes the control design challenging, and for this reason, many approaches have been proposed in the literature. Proportional–Integral–Derivative (PID) controllers have been widely investigated, as they are the most widespread controllers in industry, and, indeed, they have also been proven to be very effective in anesthesia [3–9]. Some variations of the standard PID algorithm have also been devised, including the event-based PID controller, which has been shown to be able to better mimic the behavior of the anesthesiologist [9]. In the context of PID control, a great interest is in the use of fractional-order PID (FOPID) controllers, as they provide additional flexibility in the controller design, which, in principle, should result in a better performance. Indeed, a FOPID controller has five parameters to tune: in addition to the three classic parameters (proportional gain, integral time constant and derivative time constant), the integral and derivative orders can also be freely chosen as real numbers, and this implies, for example, that a loop-shaping design can be improved. The use of fractional control in anesthesia has already been considered. In particular, a CRONE controller was first applied in [10] for DoH control, where the WAV_{CNS} system was used instead of the BIS, resulting in a high-order controller. The CRONE approach was also used in [11] for the design of a fault-tolerant control system consisting of a PID controller with a fractional-order filter. A fractional adaptive high-gain controller was proposed in [12], where the assessment of the controller performance was carried out by considering four patients. Fractional-order closed-loop model reference adaptive control was presented in [13,14], with the main aim of increasing the robustness of the system.

Regarding FOPID controllers specifically, they were employed for DoH control in [15], where the isodamping approach [16] was used to tune a FOPI controller, and the methodology was evaluated by considering 24 patients. A more general framework also involving hemodynamic variables was considered in [17,18], and the FOPID controllers were tested on the same 24 patients. Finally, a multivariable approach targeting the control of cardiac output and mean arterial pressure was presented in [19–21].

Despite some pioneering studies on the use of fractional control in anesthesia, it appears that a thorough analysis of the performance achievable with a FOPID controller and a rigorous comparison with PID controllers are still lacking. Indeed, a FOPID controller is more complex than a PID controller, and therefore, it should provide clear advantages over its integer-order counterpart to justify its adoption. In this paper, we provide such an analysis. In particular, we tuned both a PID controller and a FOPID controller by using genetic algorithms to minimize the worst-case integrated absolute error (IAE) on a dataset of 13 patients representative of a diverse population. Note that this approach has already been proven to be effective for PID controllers [3] and has also been confirmed by clinical results [22]. The obtained controllers were then tested on many virtual patients, generated with the Monte Carlo method, in order to consider both inter- and intra-patient variability. In addition, a FOPID controller was designed by also applying the isodamping approach [23] and tested on the same set of patients generated by the Monte Carlo method. In this way, the two typical options for the design of the FOPID controller were both considered.

This paper is organized as follows. The patient model, the control architectures and the design of the controllers are explained in Section 2. The extensive simulation results are presented in Section 3 and discussed in Section 4. Finally, conclusions are drawn in Section 5.

2. Materials and Methods

The aim of this paper is to compare the performance achieved by FOPID and PID controllers. To this end, it is essential to design the controllers to optimize the same functional so that the comparison is fair, which in turn requires the PK/PD model of the patient.

2.1. Patient Model

In the design of the controller, a key role is played by the model used to represent the patient during propofol administration. The well-known Schnider PK/PD model [24,25] was employed in this study. Pharmacokinetics describes the relationship between the administered drug and its plasmatic concentration, while pharmacodynamics describes the relationship between the plasmatic concentration and the clinical effect on the human body. A mammillary three-compartmental model is used for the pharmacokinetics of propofol. In this model structure, there are two peripheral compartments and a central compartment; see Figure 1. Each compartment describes cumulative volumes that have the same drug concentration. These compartments interact with each other by transferring the drug according to the following mass flow equations, which describe this exchange:

$$\begin{aligned} \dot{q}_1(t) &= -(k_{10} + k_{12} + k_{13})q_1(t) + k_{21}q_2(t) + k_{31}q_3(t) + u(t) \\ \dot{q}_2(t) &= k_{12}q_1(t) - k_{21}q_2(t) \\ \dot{q}_3(t) &= k_{13}q_1(t) - k_{31}q_3(t) \end{aligned} \tag{1}$$

where $u(t)$ (mg/min) is the drug infusion rate, $q_i(t)$ (mg) is the quantity of drug in each compartment, and k_{ij} (for $i \neq j$) (min^{-1}) represents the drug transfer frequency from the ith to the jth compartments. The output of this model is the plasmatic concentration of propofol, that is:

$$C_p(t) = \frac{q_1(t)}{V_1}, \qquad \left[\frac{\text{mg}}{\text{L}}\right] \tag{2}$$

where V_1 represents the volume of the primary compartment. The output $C_p(t)$ of the PK model is the input of the PD model, which describes the relation between the plasmatic concentration and the BIS value. A linear dynamic part relates the plasmatic concentration of propofol in the central compartment to the drug concentration in the effect-site compartment. From the metabolism in the cerebral cortex, it is possible to write:

$$\dot{C}_e(t) = k_{e0}(C_p(t) - C_e(t)), \tag{3}$$

where k_{e0} quantifies the lag time, and its estimated value is:

$$k_{e0} = 0.0495. \qquad \left[\text{min}^{-1}\right] \tag{4}$$

The last part of the PD model is an algebraic nonlinearity that describes the relationship between the effect-site concentration and the BIS value (the clinical effect of the drug). It is represented by a sigmoid curve referred to as the Hill function:

$$BIS(t) = E_0 - E_{max}\left(\frac{C_e(t)^{\gamma}}{C_{e50}^{\gamma} + C_e(t)^{\gamma}}\right), \tag{5}$$

where E_0 is the baseline effect that represents the initial drug-free state of the patient, $E_0 - E_{max}$ is the maximum achievable clinical effect, C_e is the value of the drug concentration inside the effect site, γ represents the slope of the sigmoidal curve, and C_{e50} is the drug concentration that is necessary to reach 50% of the maximal effect.

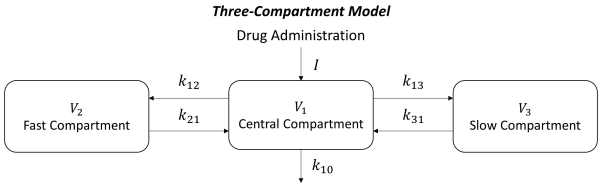

Figure 1. Schematic of the pharmacokinetics compartmental model.

2.2. PID Controller

The (standard) PID control scheme that is considered in this paper is shown in Figure 2. The PID controller is in ideal form; that is, its transfer function is

$$C(s) = K_p\left(1 + \frac{1}{T_i s} + \frac{T_d s}{\frac{T_d}{N}s + 1}\right), \tag{6}$$

where K_p is the proportional gain, T_i is the integral time constant, and T_d is the derivative action time constant. The derivative action is filtered by using a first-order system with $N = 5$ [26]. Further, an anti-windup back-calculation strategy (where $T_t = \sqrt{T_i T_d}$ is the tracking time constant) is employed [26]. The use of anti-windup is necessary to handle the actuator saturation. It is easily understandable that clinical syringe pumps cannot have a negative infusion rate, and thus, the lower saturation limit is set to 0. The upper saturation limit depends on the type of infusion pump used since the rate is related to the syringe size. In this work, the specifications of a Graseby™ 3500 pump were used to model the surgical equipment available in a typical surgery room. Accordingly, the maximum flow rate of 1200 (mL/h) was set, resulting in a maximum infusion rate of 6.67 (mg/s) by considering a propofol concentration of 20 (mg/mL).

The controller was tuned by minimizing the worst-case integrated absolute error (IAE) for a specific set of 13 patients representative of a diverse population; see [3,27] for the details of the patient demographics. The IAE is defined as

$$IAE = \int_0^\infty |BIS(t) - r(t)|dt, \tag{7}$$

where $BIS(t)$ is the the value of the BIS signal of the patient at time t, and $r(t) = 50$ is its reference value. The optimization problem was solved in MATLAB by using genetic algorithms with a population size of 100. A Gaussian mutation was used to add a random number taken from a Gaussian distribution with mean 0 to each entry of the parent vector, thus resulting in the random perturbation of the individuals that will belong to the future generation. Furthermore, a scattered crossover was employed to create a random binary vector. The genetic algorithm selects hereditary genes from the first parent when the random vector element is a 1 and genes from the second parent where the vector has a 0. Then, the selected genes are combined to form the child. The resulting optimal values of K_p, T_i, T_d and T_t are shown in Table 1.

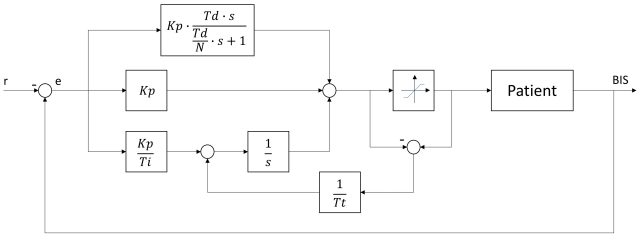

Figure 2. PID−based control structure.

Table 1. Tuning parameters for each controller. Note that for the isodamping scenarios (ISO), the value of T_t is computed as $\sqrt{T_i T_d}$. The worst-case IAE achieved on the 13 patients is shown in the IAE column.

Controller	K_p	T_i	T_d	T_t	λ	μ	IAE
PID	0.0458	156.4	22.34	84.44	-	-	1685.2
FOPID IAE	0.0393	59.56	22.94	89.96	0.8467	0.7978	1531.3
FOPID ISO1	0.2053	207.1	13.01	51.90	0.1136	1.005	1695.9
FOPID ISO2	0.0552	373.9	30.34	106.5	0.9994	1.2084	2354.1

2.3. FOPID Controller

The transfer function of the FOPID controller is

$$C(s) = K_p\left(1 + \frac{1}{T_i s^{\lambda}} + \frac{T_d s^{\mu}}{\frac{T_d}{N^{\mu}} s^{\mu} + 1}\right), \tag{8}$$

where λ and μ are the fractional-order terms of the integral and derivative actions, respectively. These new parameters introduce, compared to the PID controller, additional design flexibility, which can be exploited to improve the robustness/performance trade-off. Looking at the control scheme shown in Figure 3, it is possible to see that a back-calculation anti-windup technique has been implemented in this case, as well [28]. The advantage of the back-calculation approach is that it relies on the integrator's own dynamics, thereby making it suitable for PID and FOPID alike.

To implement a fractional-order controller, it is necessary to approximate the non-integer-order part with a transfer function that consists of a series of zeros and poles of integer order. In this context, the CRONE approximation [29] was used with 8 pairs of poles and zeros and within a range of frequencies from 10^{-4} to 10 (rad/s).

Two different methods were employed to tune the FOPID controller. In the first case, the FOPID controller was tuned by applying the same methodology employed for the PID controller, namely, by minimizing the worst-case IAE for the set of 13 patients. The second method exploits the isodamping property. This approach consists of flattening the phase at the gain crossover frequency to guarantee zero phase margin variations with respect to changes in the process dc gain [23]. In this context, a nominal process model is needed to design the controller. The demographic values of the thirteenth patient in the previously mentioned database were used as a reference. Moreover, the model nonlinearity, i.e., the Hill function, was linearized around a BIS value of 50. Thus, the process can be written as:

$$P(s) = K\frac{\left(\frac{s}{z_1}+1\right)\left(\frac{s}{z_2}+1\right)}{\left(\frac{s}{p_1}+1\right)\left(\frac{s}{p_2}+1\right)\left(\frac{s}{p_3}+1\right)\left(\frac{s}{p_4}+1\right)}, \tag{9}$$

where z_1, z_2 and p_1, p_2, p_3 are the zeroes and poles that come from the PK model, p_4 is the pole deriving from the PD model, and K is the product of the dc gains of the PK model, the PD model and the slope of the Hill function at $BIS = 50$. More precisely, the linearized Hill function is

$$K_{Hill} = E_{max}\left[\frac{\gamma Ce_{ref}^{\gamma-1} Ce_{50}^{\gamma}}{\left(Ce_{ref}^{\gamma} + Ce_{50}^{\gamma}\right)^2}\right], \tag{10}$$

where Ce_{ref} is the drug concentration value in the patient that produces a BIS equal to 50, and it is calculated as follows:

$$Ce_{ref} = \left[\frac{Ce_{50}^{\gamma}(E_0 - 50)}{E_{max} + 50 - E_0}\right]^{1/\gamma}. \tag{11}$$

The values of E_0, E_{max}, Ce_{50} and γ were taken from [30]. The optimal controller parameters were then determined by solving an optimization problem that minimizes the maximum sensitivity M_s, defined as

$$M_s := \max_{\omega} |S(j\omega)| = \max_{\omega} \left| \frac{1}{1 + C(j\omega)P(j\omega)} \right|, \tag{12}$$

subject to the following frequency constraints:

- $\omega_c = \bar{\omega}_c$ (desired gain crossover frequency);
- $\phi_m = \bar{\phi}_m$ (desired phase margin);
- $\frac{d\phi_m}{dx} = 0$ (isodamping condition).

Two sets of values of $\bar{\omega}_c$ and $\bar{\phi}_m$ were selected (thus obtaining two sets of optimal FOPID parameters). These sets were determined by considering the frequency response of the loop transfer function $L(s) = C(s)P(s)$, where each of the linearized models of the 13 patients is in series with either the PID controller tuned with the optimization method described in Section 2.2 or the PID controller presented in [7], where an individualized approach is employed. In particular, for each of the 13 patients, the values of the gain crossover frequency and of the phase margin were determined, and the resulting average values were used as constraints in the isodamping optimization problem. The first case (from the PID controller in Section 2.2) is denoted by ISO1 and has $\bar{\omega}_c = 0.08$ (rad/s) and $\bar{\phi}_m = 57.5°$. The second case (from the PID controller designed in [7]) is denoted by ISO2 and consists of $\bar{\omega}_c = 0.03$ (rad/s) and $\bar{\phi}_m = 65°$. Note that the second set should provide a slower and more robust controller. In fact, from the first set, a worst-case maximum sensitivity of 1.204 is obtained, while using the second set of constraints yields $M_s = 1.053$. Indeed, two different design options were considered in order to thoroughly evaluate the effectiveness of the isodamping approach in different contexts. Genetic algorithms were also exploited in this case to solve the optimization problem. However, in this scenario, the problem is subject to some equality constraints, which causes genetic algorithms to solve many subproblems at each iteration. For this purpose, the default mutation function 'mutationadaptfeasible' for constrained GA problems was used. This function randomly generates directions that are adaptive with respect to the last successful or unsuccessful generation. The mutation chooses a direction and step length that satisfy bounds and linear constraints. A constraint tolerance equal to 1×10^{-4} was used. The resulting optimal values of the controller parameters are shown in Table 1. Note that N is fixed to 5 for all controllers and all design procedures.

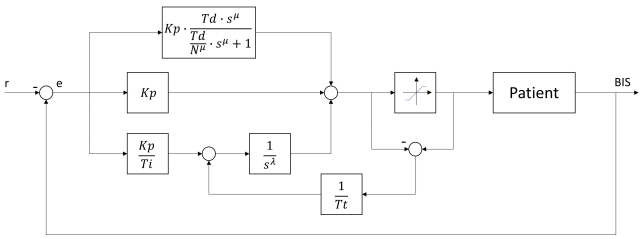

Figure 3. FOPID−based control structure.

3. Results

In this section, the simulation results are presented. It was decided to simulate a maintenance phase of 50 min. During this time interval, the control task is to maintain the BIS level at the desired set-point value. The double-step signal proposed in [31] was exploited to model the external stimuli coming from the surgery. In particular, a positive-step signal (at the 10th minute) with an amplitude of 10 is followed, after 20 min, by a negative step with the same amplitude.

Initially, the 13 patients in the design database were analyzed. Figure 4 shows the responses obtained by the PID and FOPID controllers, both tuned by minimizing the IAE. In this scenario, the two controllers perform in a similar way in rejecting both the positive

and negative steps. A marginal difference can be found in the positive-step rejection, with the FOPID controller being slightly faster compared to the PID controller, while the two behave in virtually the same way with the negative step. Figure 5 presents the results obtained with the FOPID tuned with the isodamping approach, where the maximum sensitivity is minimized subject to a gain crossover frequency of 0.08 (rad/s) and a desired phase margin of 57.5° (ISO1). The performance of the PID and FOPID controllers is different, with the FOPID providing a faster transient response but also having a more pronounced undershoot. This is mainly due to the larger value of the proportional gain K_p; see Table 1. This behavior is also noticeable in the rejection of the negative step. Here, however, the FOPID is again faster, but the overshoot is minimal, leading to an overall much better transient response.

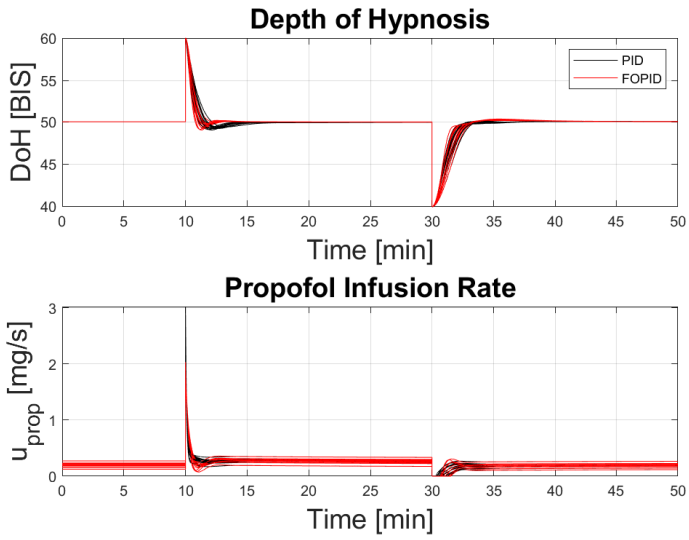

Figure 4. Simulation responses obtained with the 13 patients used in the tuning procedure. Black solid line: PID controller. Red solid line: FOPID controller.

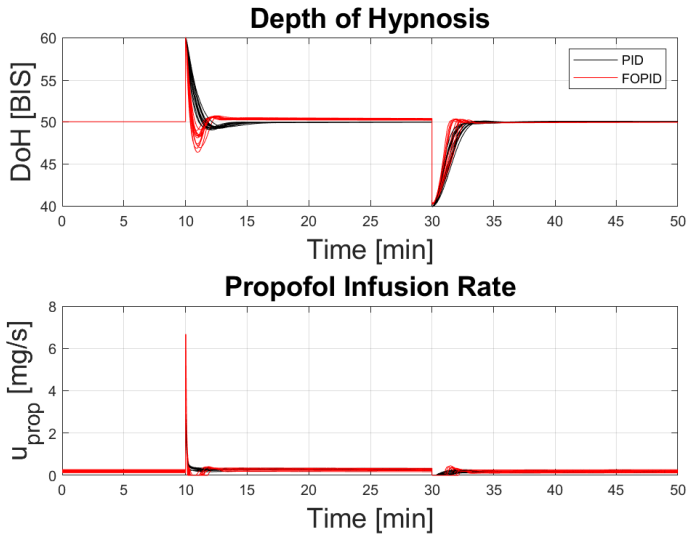

Figure 5. Simulation responses obtained with the 13 patients used in the tuning procedure. Black solid line: PID controller. Red solid line: FOPID ISO1 controller.

Figure 6 shows the responses obtained with the FOPID tuned by applying the isodamping approach subject to a gain crossover frequency of 0.03 (rad/s) and a phase margin of 65° (ISO2) (again, in comparison with the PID controller). The PID and the FOPID provide more or less the same performance in rejecting the positive step. Conversely, the controllers have different behaviors in rejecting the negative disturbance. Here, the FOPID

presents a slower and a more damped transient response with respect to the PID, causing a delay in reaching the steady-state value. All these considerations are confirmed by the performance indices proposed in [27], i.e.,

- Time to Target (TT): the time interval required for the BIS value to enter the range of $50 \pm 10\%$ for the first time;
- BIS-NADIR: the lowest or highest BIS value reached during the whole control interval for a positive or negative step, respectively.

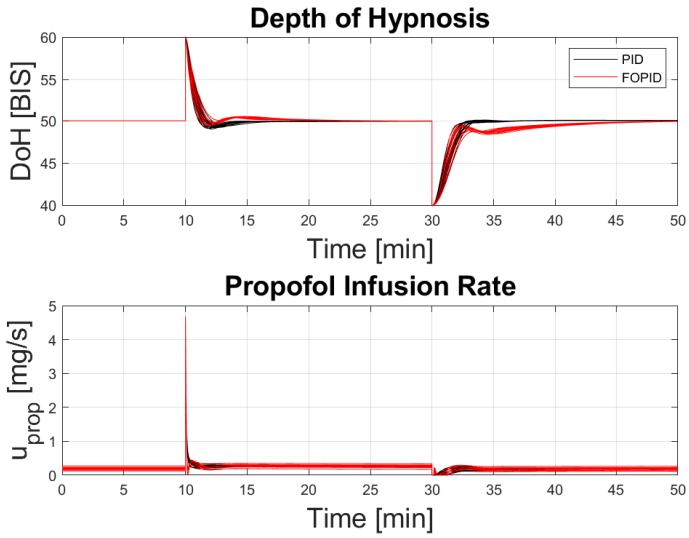

Figure 6. Simulation responses obtained with the 13 patients used in the tuning procedure. Black solid line: PID controller. Red solid line: FOPID ISO2 controller.

Figures 7 and 8 show the Time-to-Target boxplot for each controller. The FOPID ISO1 (yellow box), since it is more aggressive, is faster compared to the others in rejecting disturbances. However, looking at Figures 9 and 10, this controller presents more pronounced undershoots and overshoots. The performance provided by the other three controllers is very similar when rejecting both the positive and negative steps. Overall, it can be concluded that all the controllers satisfy the clinical requirements and that there are no major differences between them.

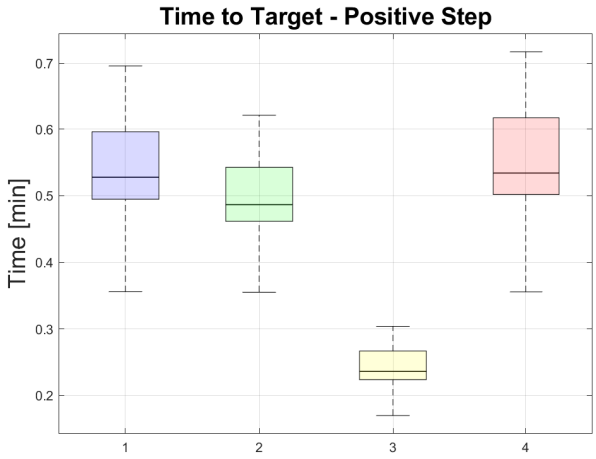

Figure 7. Time-to-Target indices for each controller with a positive step. (1) Blue box: PID controller. (2) Green box: FOPID IAE. (3) Yellow box: FOPID ISO1. (4) Red box: FOPID ISO2.

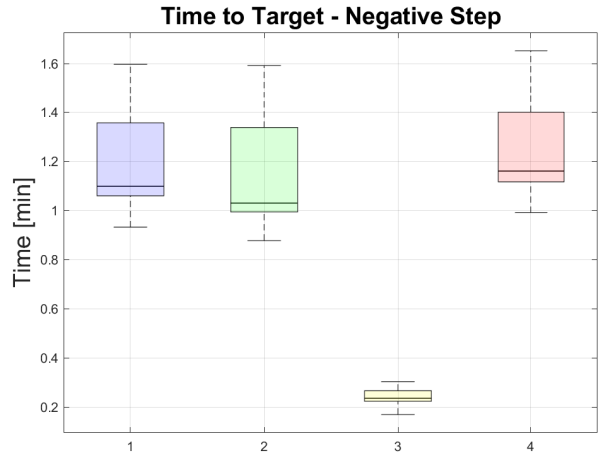

Figure 8. Time-to-Target indices for each controller with a negative step. (1) Blue box: PID controller. (2) Green box: FOPID IAE. (3) Yellow box: FOPID ISO1. (4) Red box: FOPID ISO2.

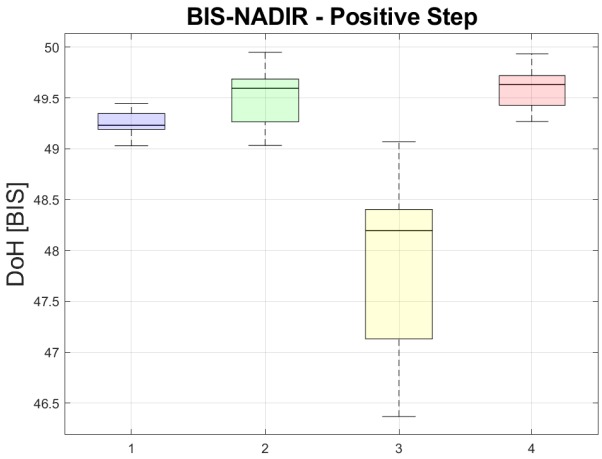

Figure 9. BIS-NADIR indices for each controller with a positive step. (1) Blue box: PID controller. (2) Green box: FOPID IAE. (3) Yellow box: FOPID ISO1. (4) Red box: FOPID ISO2.

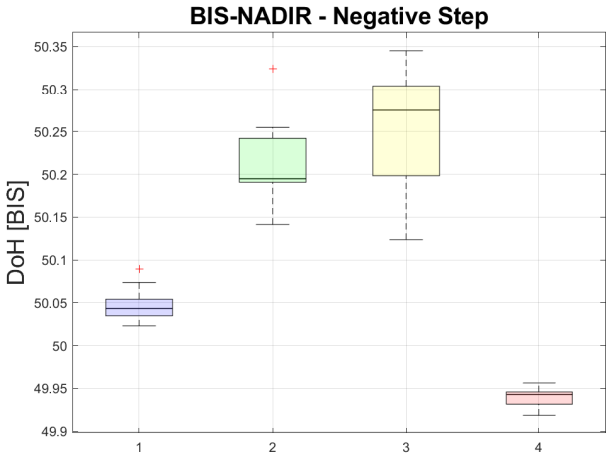

Figure 10. BIS-NADIR indices for each controller with a negative step. (1) Blue box: PID controller. (2) Green box: FOPID IAE. (3) Yellow box: FOPID ISO1. (4) Red box: FOPID ISO2. Outliers are marked with red crosses.

In order to provide a more rigorous comparison, the controllers were tested on a much larger population of patients than the 13 individuals used for the design. New patients were generated through the Monte Carlo method presented in [7], and both inter-patient and intra-patient variabilities were considered. In particular, a set of 500 patients with different demographic data was created to study inter-patient variability. Further, 500 patients with different model parameters were generated from each of the 13 patients in the original database to investigate intra-patient variability. Hence, a diverse set totaling 6500 patients was used to analyze the performance of the controllers.

Figure 11 shows the comparison between the PID and the FOPID, both tuned by minimizing the IAE. The FOPID controller presents a slightly larger undershoot in the positive-step rejection. As expected, the performance is virtually the same in rejecting the negative step. The results obtained with the FOPID ISO1 are shown in Figure 12. In this scenario, the results again confirm that the controller is more aggressive and a larger undershoot occurs. In fact, this controller is less robust than the others. Figure 13 shows the results obtained with the FOPID ISO2. Here, the issues in the rejection of the negative step are present again. It is important to underline that the proposed control solution meets the control system requirements for each of the 500 patients. On average, all the designed controllers demonstrate a satisfactory robustness to inter-patient variability, as clinical requirements are always met. This is confirmed by the performance indices shown in Figures 14–17.

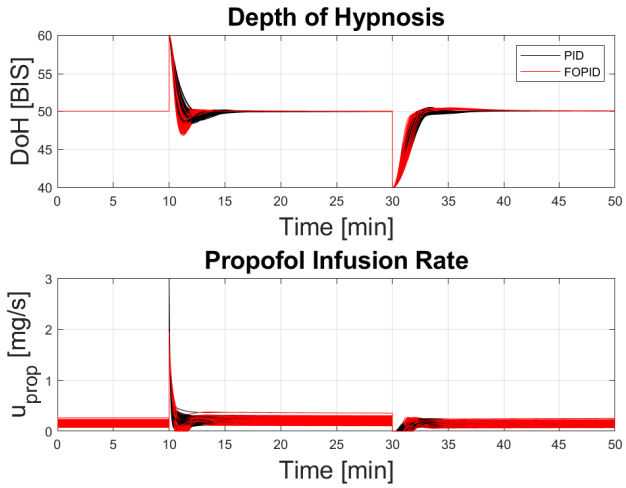

Figure 11. Simulation responses obtained on the 500 patients to study inter-patient variability. Black solid line: PID controller. Red solid line: FOPID IAE controller.

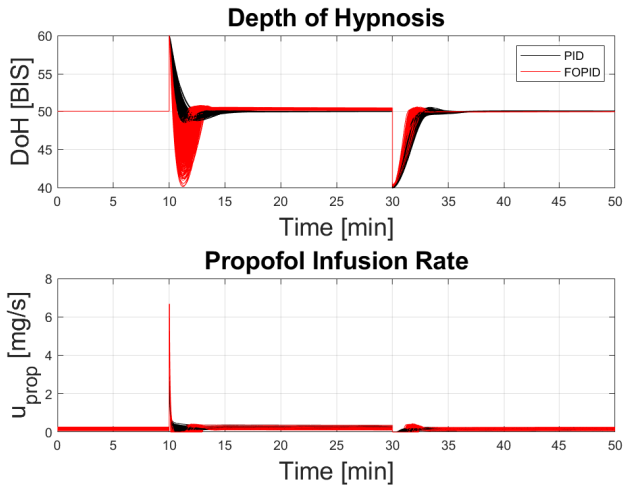

Figure 12. Simulation responses obtained on the 500 patients to study inter-patient variability. Black solid line: PID controller. Red solid line: FOPID ISO1 controller.

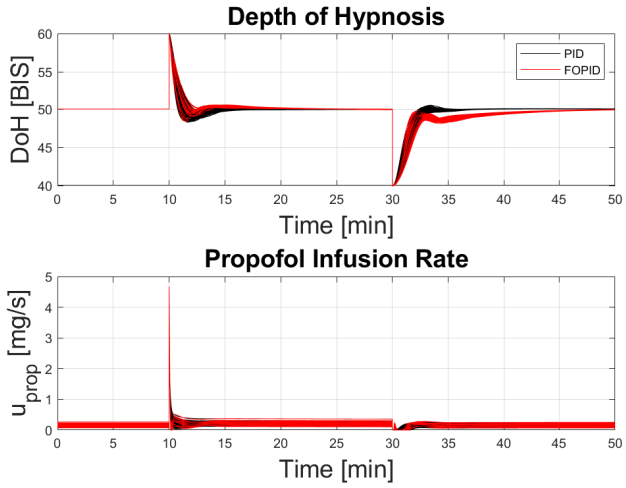

Figure 13. Simulation responses obtained on the 500 patients to study inter-patient variability. Black solid line: PID controller. Red solid line: FOPID ISO2 controller.

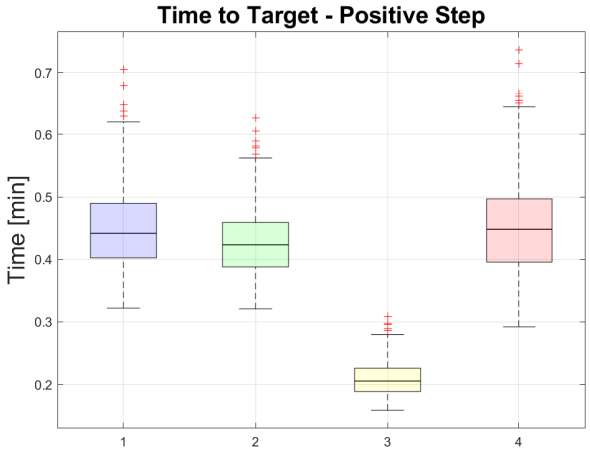

Figure 14. Time-to-Target indices for each controller when a positive step occurs. (1) Blue box: PID controller. (2) Green box: FOPID IAE. (3) Yellow box: FOPID ISO1. (4) Red box: FOPID ISO2. Outliers are marked with red crosses.

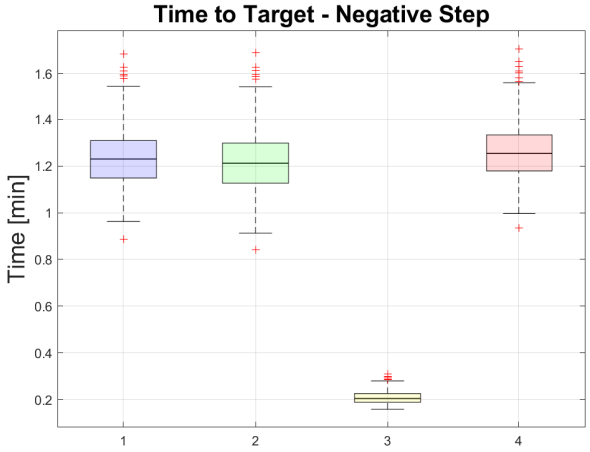

Figure 15. Time-to-Target indices for each controller when a negative step occurs. (1) Blue box: PID controller. (2) Green box: FOPID IAE. (3) Yellow box: FOPID ISO1. (4) Red box: FOPID ISO2. Outliers are marked with red crosses.

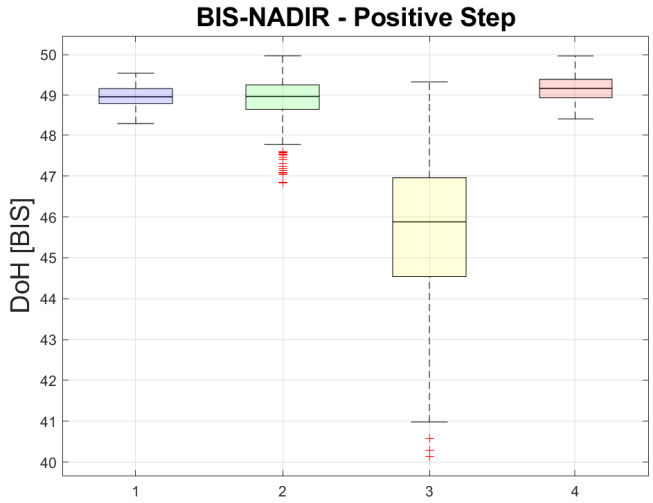

Figure 16. BIS-NADIR indices for each controller when a positive step occurs. (1) Blue box: PID controller. (2) Green box: FOPID IAE. (3) Yellow box: FOPID ISO1. (4) Red box: FOPID ISO2. Outliers are marked with red crosses.

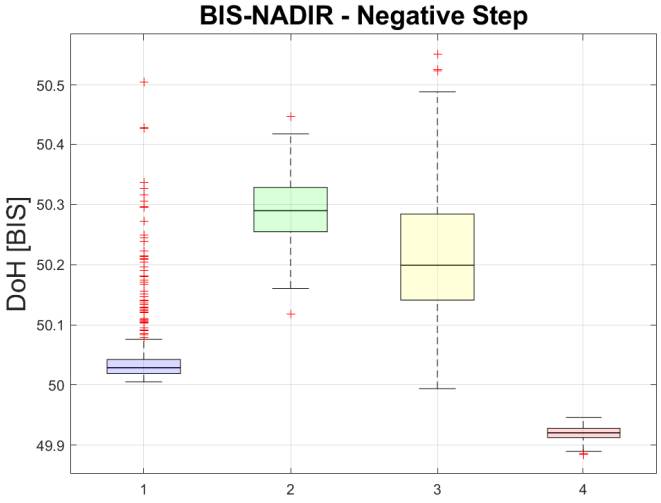

Figure 17. BIS-NADIR indices for each controller when a negative step occurs. (1) Blue box: PID controller. (2) Green box: FOPID IAE. (3) Yellow box: FOPID ISO1. (4) Red box: FOPID ISO2. Outliers are marked with red crosses.

Finally, the performance indices related to intra-patient variability are shown (for each patient) in Figures 18–69. Plots of the disturbance responses are omitted for brevity. The same considerations of the inter-patient variability apply to intra-patient variability. The consistency between inter- and intra-patient variability analysis and the results obtained with the design set of 13 individuals also confirms that the set used in the design phase is indeed a representative sample of a diverse population.

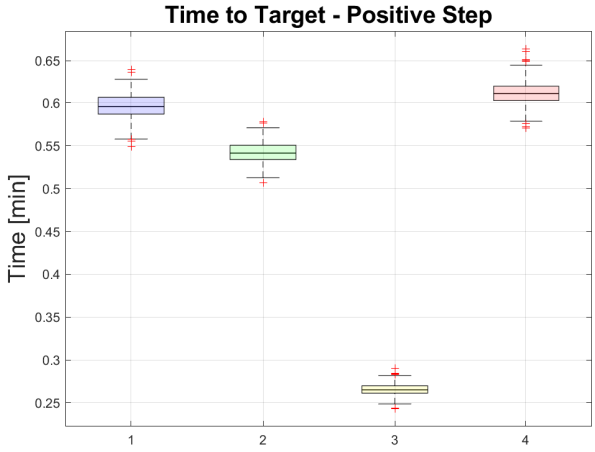

Figure 18. Intra-patient robustness of patient 1. Positive-step Time-to-Target indices for each controller. (1) Blue box: PID controller. (2) Green box: FOPID IAE. (3) Yellow box: FOPID ISO1. (4) Red box: FOPID ISO2. Outliers are marked with red crosses.

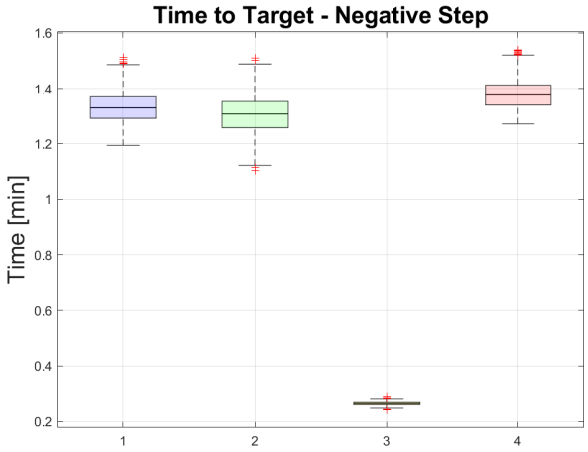

Figure 19. Intra-patient robustness of patient 1. Negative-step Time-to-Target indices for each controller. (1) Blue box: PID controller. (2) Green box: FOPID IAE. (3) Yellow box: FOPID ISO1. (4) Red box: FOPID ISO2. Outliers are marked with red crosses.

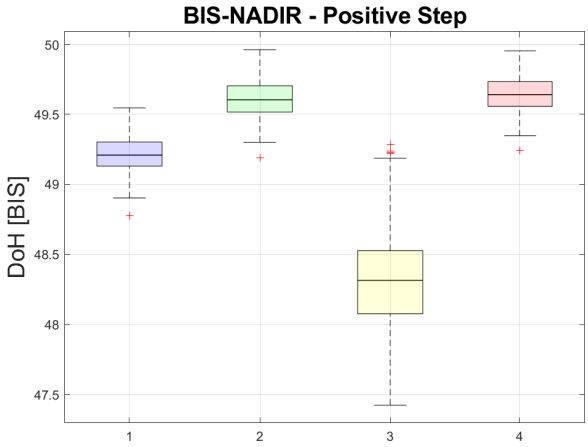

Figure 20. Intra-patient robustness of patient 1. Positive-step BIS-NADIR indices for each controller. (1) Blue box: PID controller. (2) Green box: FOPID IAE. (3) Yellow box: FOPID ISO1. (4) Red box: FOPID ISO2. Outliers are marked with red crosses.

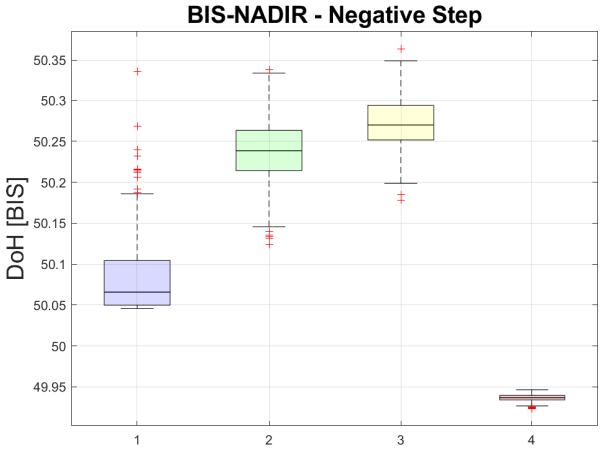

Figure 21. Intra-patient robustness of patient 1. Negative-step BIS-NADIR indices for each controller. (1) Blue box: PID controller. (2) Green box: FOPID IAE. (3) Yellow box: FOPID ISO1. (4) Red box: FOPID ISO2. Outliers are marked with red crosses.

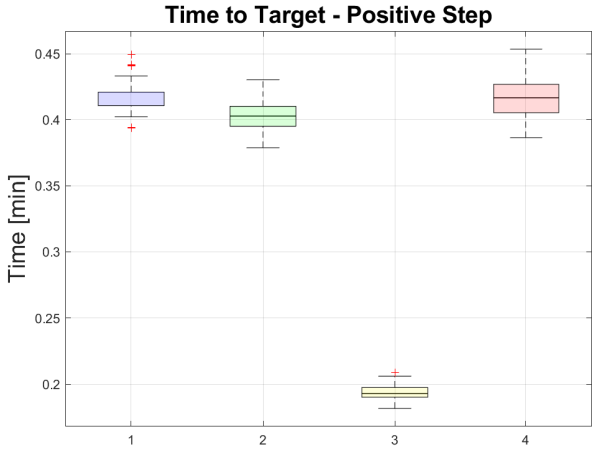

Figure 22. Intra-patient robustness of patient 2. Positive-step Time-to-Target indices for each controller. (1) Blue box: PID controller. (2) Green box: FOPID IAE. (3) Yellow box: FOPID ISO1. (4) Red box: FOPID ISO2. Outliers are marked with red crosses.

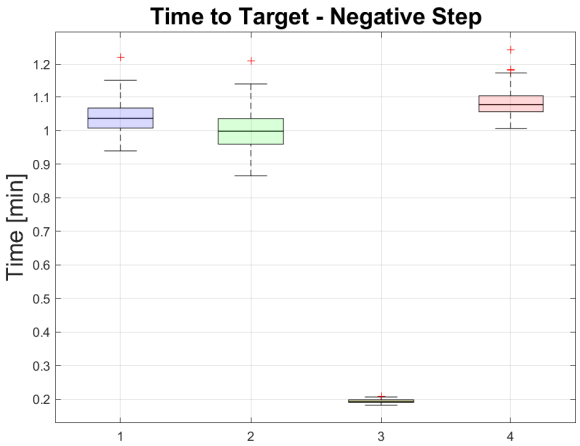

Figure 23. Intra-patient robustness of patient 2. Negative-step Time-to-Target indices for each controller. (1) Blue box: PID controller. (2) Green box: FOPID IAE. (3) Yellow box: FOPID ISO1. (4) Red box: FOPID ISO2. Outliers are marked with red crosses.

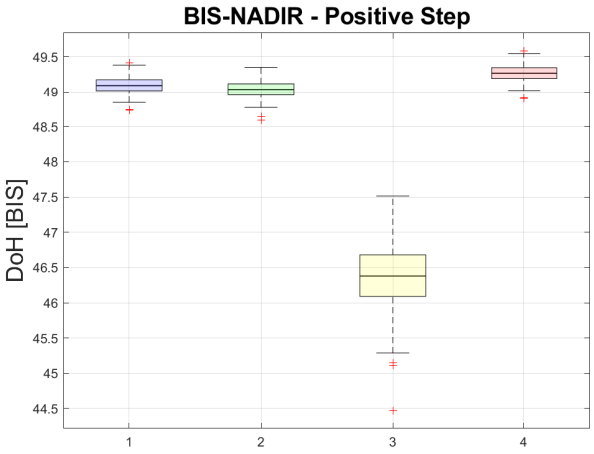

Figure 24. Intra-patient robustness of patient 2. Positive-step BIS-NADIR indices for each controller. (1) Blue box: PID controller. (2) Green box: FOPID IAE. (3) Yellow box: FOPID ISO1. (4) Red box: FOPID ISO2. Outliers are marked with red crosses.

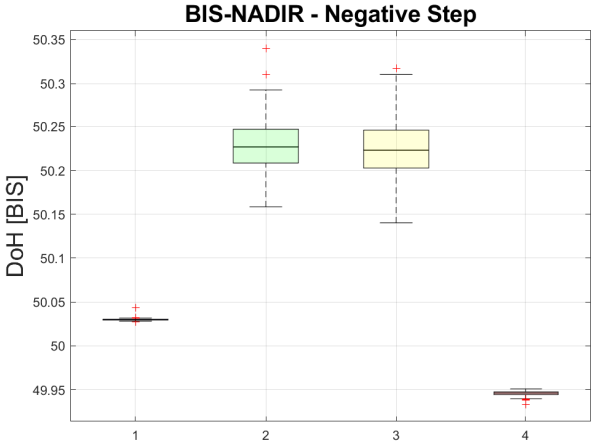

Figure 25. Intra-patient robustness of patient 2. Negative-step BIS-NADIR indices for each controller. (1) Blue box: PID controller. (2) Green box: FOPID IAE. (3) Yellow box: FOPID ISO1. (4) Red box: FOPID ISO2. Outliers are marked with red crosses.

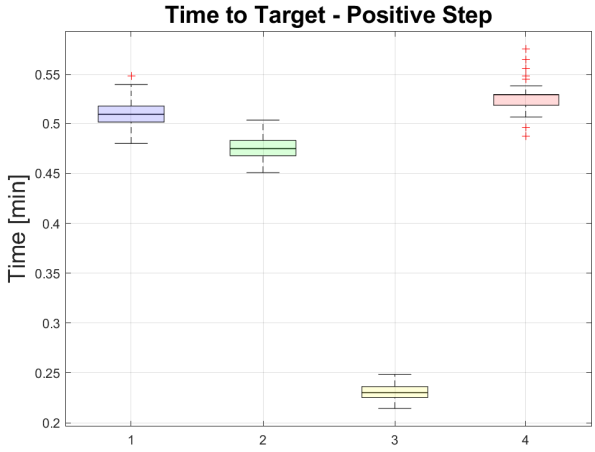

Figure 26. Intra-patient robustness of patient 3. Positive-step Time-to-Target indices for each controller. (1) Blue box: PID controller. (2) Green box: FOPID IAE. (3) Yellow box: FOPID ISO1. (4) Red box: FOPID ISO2. Outliers are marked with red crosses.

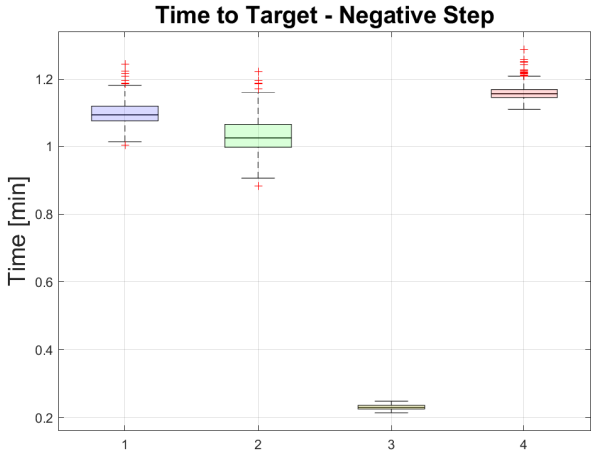

Figure 27. Intra-patient robustness of patient 3. Negative-step Time-to-Target indices for each controller. (1) Blue box: PID controller. (2) Green box: FOPID IAE. (3) Yellow box: FOPID ISO1. (4) Red box: FOPID ISO2. Outliers are marked with red crosses.

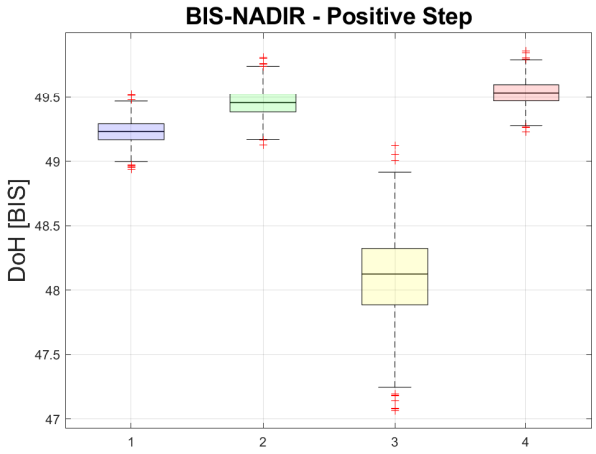

Figure 28. Intra-patient robustness of patient 3. Positive-step BIS-NADIR indices for each controller. (1) Blue box: PID controller. (2) Green box: FOPID IAE. (3) Yellow box: FOPID ISO1. (4) Red box: FOPID ISO2. Outliers are marked with red crosses.

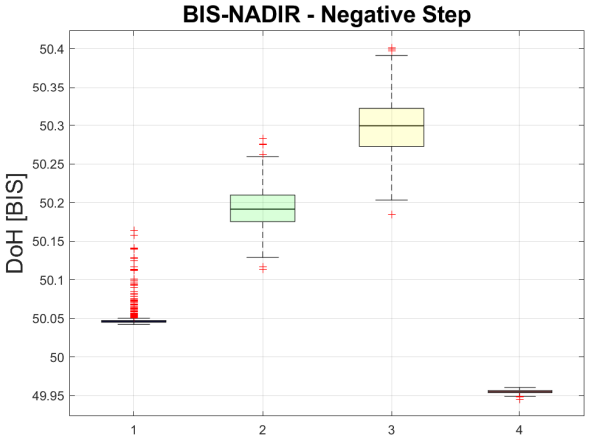

Figure 29. Intra-patient robustness of patient 3. Negative-step BIS-NADIR indices for each controller. (1) Blue box: PID controller. (2) Green box: FOPID IAE. (3) Yellow box: FOPID ISO1. (4) Red box: FOPID ISO2. Outliers are marked with red crosses.

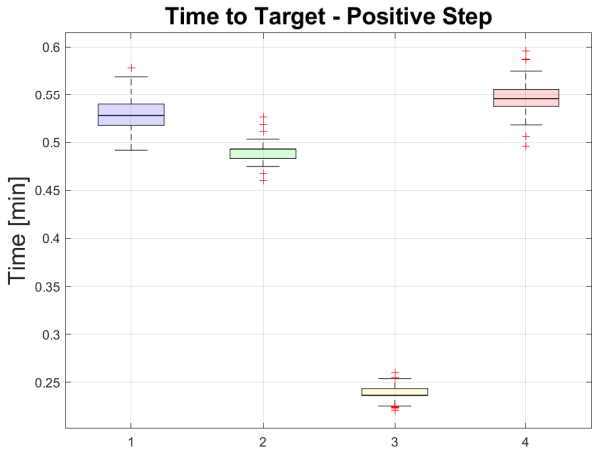

Figure 30. Intra-patient robustness of patient 4. Positive-step Time-to-Target indices for each controller. (1) Blue box: PID controller. (2) Green box: FOPID IAE. (3) Yellow box: FOPID ISO1. (4) Red box: FOPID ISO2. Outliers are marked with red crosses.

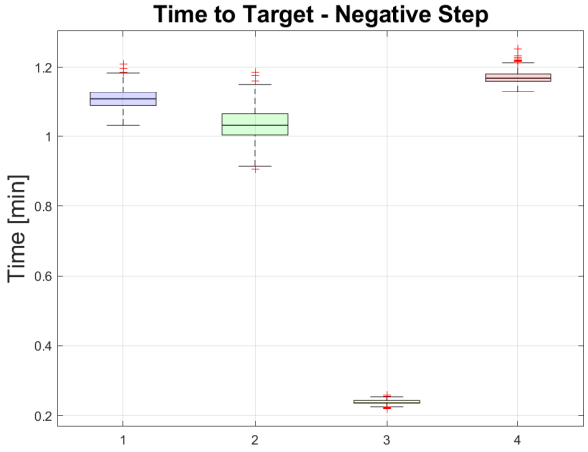

Figure 31. Intra-patient robustness of patient 4. Negative-step Time-to-Target indices for each controller. (1) Blue box: PID controller. (2) Green box: FOPID IAE. (3) Yellow box: FOPID ISO1. (4) Red box: FOPID ISO2. Outliers are marked with red crosses.

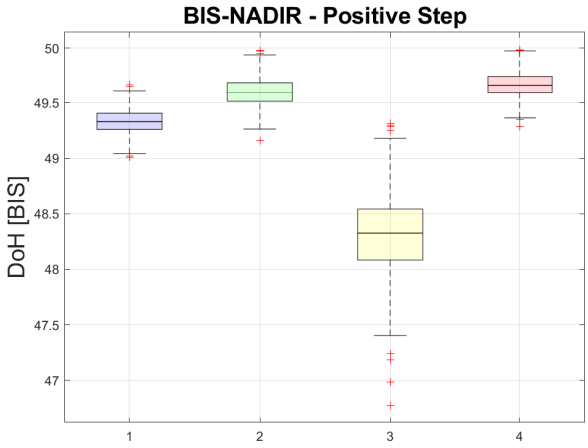

Figure 32. Intra-patient robustness of patient 4. Positive-step BIS-NADIR indices for each controller. (1) Blue box: PID controller. (2) Green box: FOPID IAE. (3) Yellow box: FOPID ISO1. (4) Red box: FOPID ISO2. Outliers are marked with red crosses.

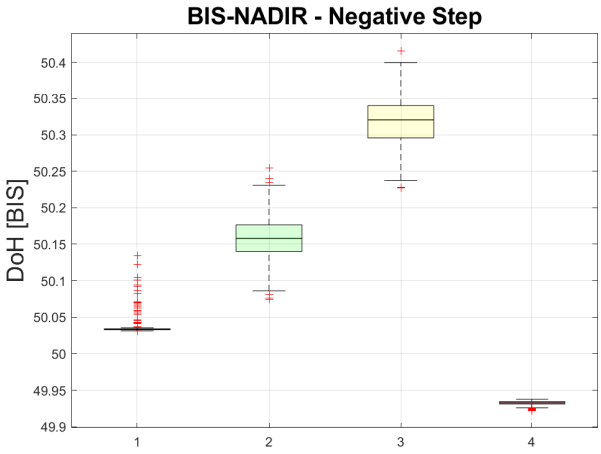

Figure 33. Intra-patient robustness of patient 4. Negative-step BIS-NADIR indices for each controller. (1) Blue box: PID controller. (2) Green box: FOPID IAE. (3) Yellow box: FOPID ISO1. (4) Red box: FOPID ISO2. Outliers are marked with red crosses.

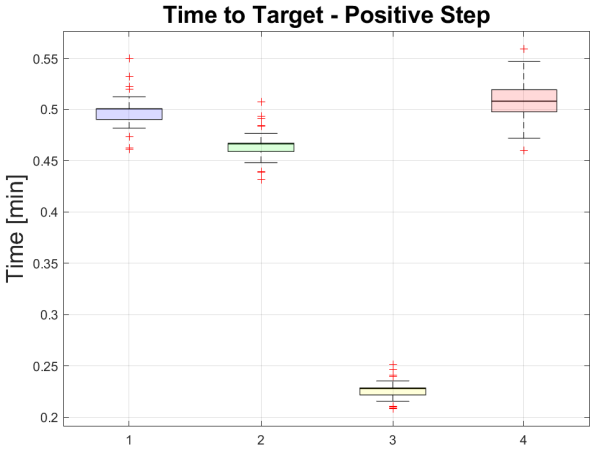

Figure 34. Intra-patient robustness of patient 5. Positive-step Time-to-Target indices for each controller. (1) Blue box: PID controller. (2) Green box: FOPID IAE. (3) Yellow box: FOPID ISO1. (4) Red box: FOPID ISO2. Outliers are marked with red crosses.

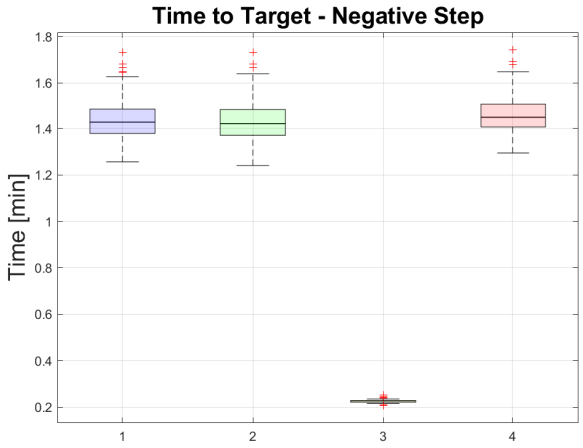

Figure 35. Intra-patient robustness of patient 5. Negative-step Time-to-Target indices for each controller. (1) Blue box: PID controller. (2) Green box: FOPID IAE. (3) Yellow box: FOPID ISO1. (4) Red box: FOPID ISO2. Outliers are marked with red crosses.

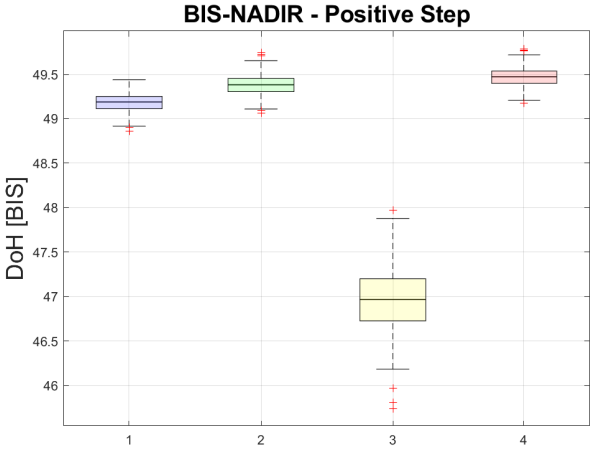

Figure 36. Intra-patient robustness of patient 5. Positive-step BIS-NADIR indices for each controller. (1) Blue box: PID controller. (2) Green box: FOPID IAE. (3) Yellow box: FOPID ISO1. (4) Red box: FOPID ISO2. Outliers are marked with red crosses.

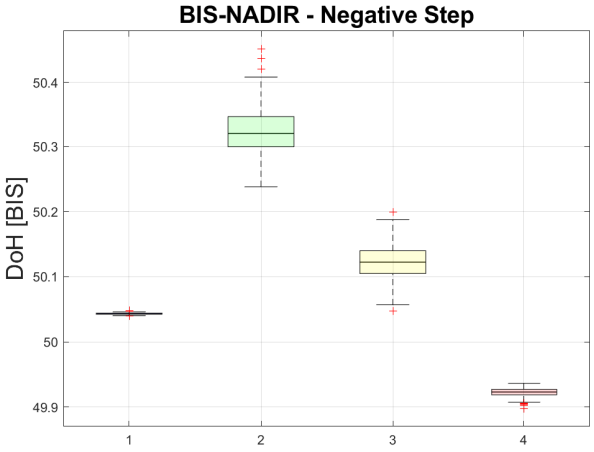

Figure 37. Intra-patient robustness of patient 5. Negative-step BIS-NADIR indices for each controller. (1) Blue box: PID controller. (2) Green box: FOPID IAE. (3) Yellow box: FOPID ISO1. (4) Red box: FOPID ISO2. Outliers are marked with red crosses.

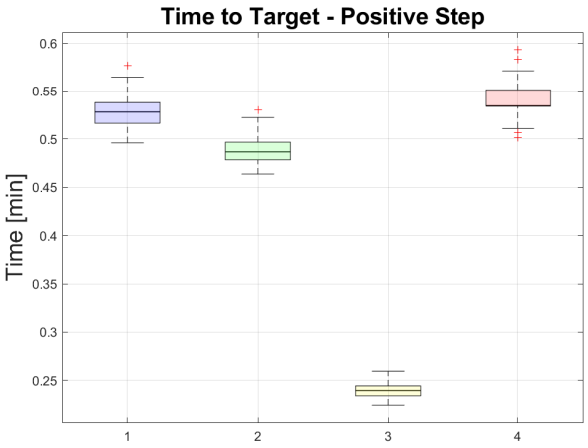

Figure 38. Intra-patient robustness of patient 6. Positive-step Time-to-Target indices for each controller. (1) Blue box: PID controller. (2) Green box: FOPID IAE. (3) Yellow box: FOPID ISO1. (4) Red box: FOPID ISO2. Outliers are marked with red crosses.

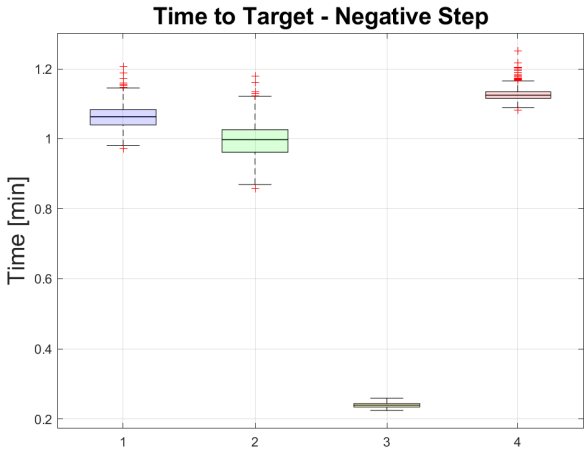

Figure 39. Intra-patient robustness of patient 6. Negative-step Time-to-Target indices for each controller. (1) Blue box: PID controller. (2) Green box: FOPID IAE. (3) Yellow box: FOPID ISO1. (4) Red box: FOPID ISO2. Outliers are marked with red crosses.

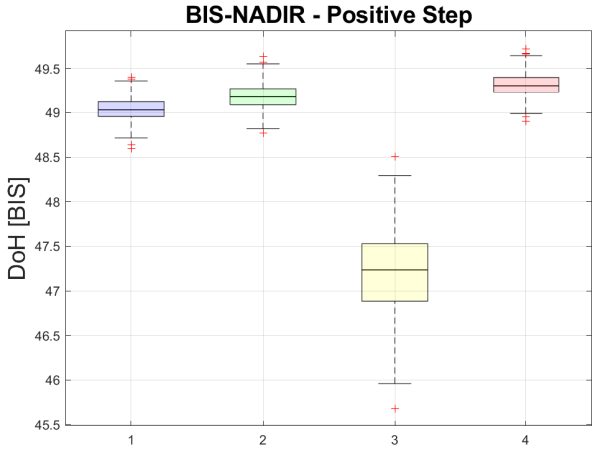

Figure 40. Intra-patient robustness of patient 6. Positive-step BIS-NADIR indices for each controller. (1) Blue box: PID controller. (2) Green box: FOPID IAE. (3) Yellow box: FOPID ISO1. (4) Red box: FOPID ISO2. Outliers are marked with red crosses.

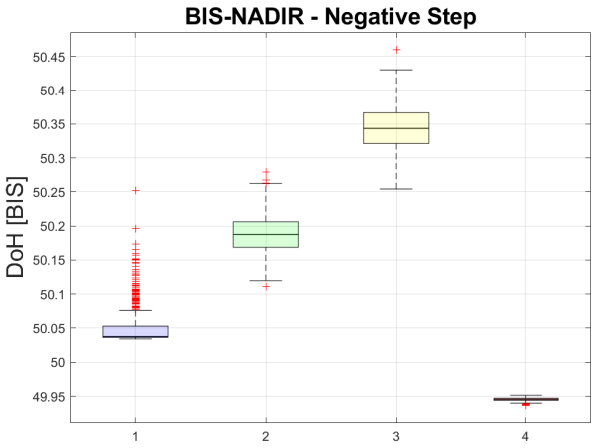

Figure 41. Intra-patient robustness of patient 6. Negative-step BIS-NADIR indices for each controller. (1) Blue box: PID controller. (2) Green box: FOPID IAE. (3) Yellow box: FOPID ISO1. (4) Red box: FOPID ISO2. Outliers are marked with red crosses.

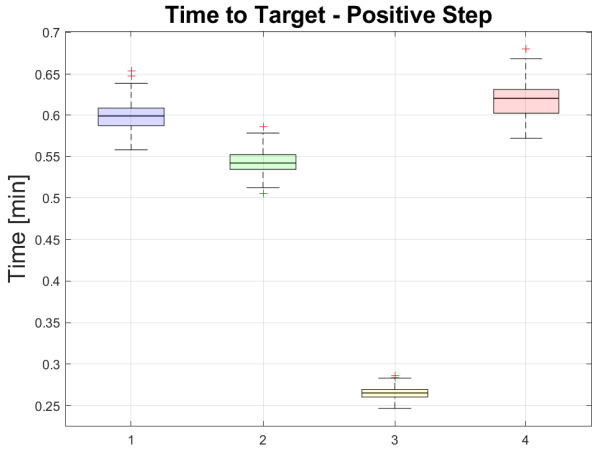

Figure 42. Intra-patient robustness of patient 7. Positive-step Time-to-Target indices for each controller. (1) Blue box: PID controller. (2) Green box: FOPID IAE. (3) Yellow box: FOPID ISO1. (4) Red box: FOPID ISO2. Outliers are marked with red crosses.

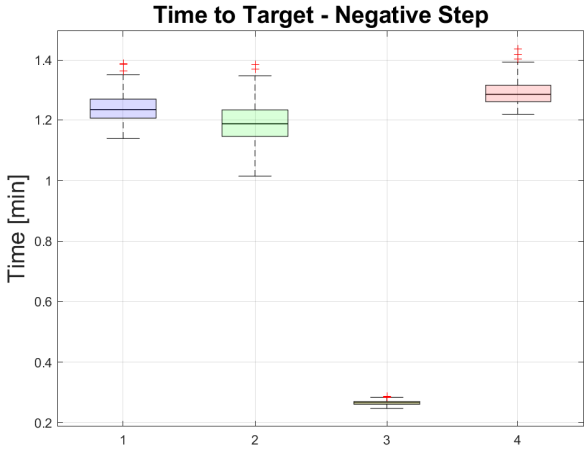

Figure 43. Intra-patient robustness of patient 7. Negative-step Time-to-Target indices for each controller. (1) Blue box: PID controller. (2) Green box: FOPID IAE. (3) Yellow box: FOPID ISO1. (4) Red box: FOPID ISO2. Outliers are marked with red crosses.

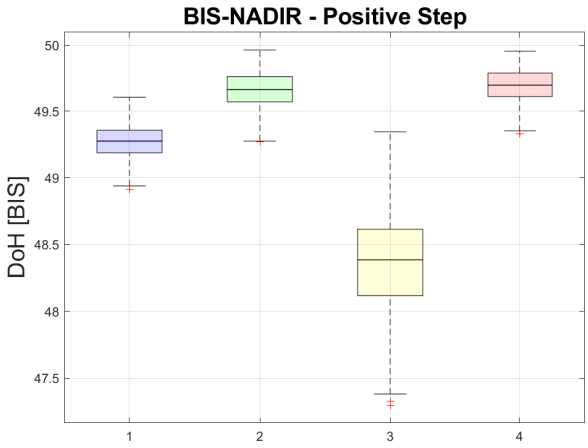

Figure 44. Intra-patient robustness of patient 7. Positive-step BIS-NADIR indices for each controller. (1) Blue box: PID controller. (2) Green box: FOPID IAE. (3) Yellow box: FOPID ISO1. (4) Red box: FOPID ISO2. Outliers are marked with red crosses.

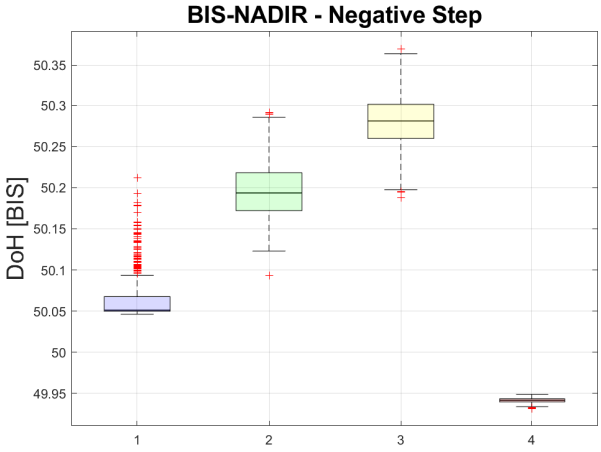

Figure 45. Intra-patient robustness of patient 7. Negative-step BIS-NADIR indices for each controller. (1) Blue box: PID controller. (2) Green box: FOPID IAE. (3) Yellow box: FOPID ISO1. (4) Red box: FOPID ISO2. Outliers are marked with red crosses.

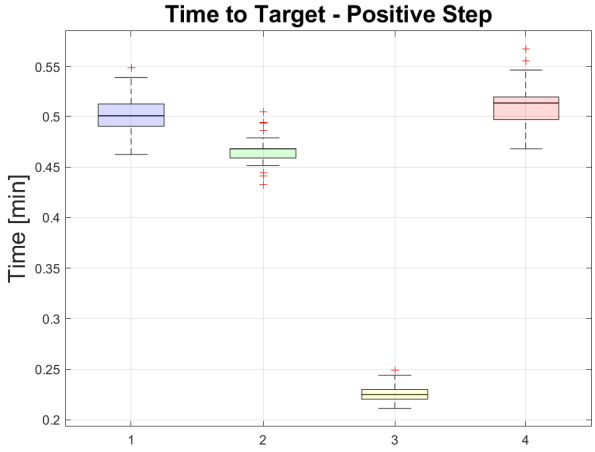

Figure 46. Intra-patient robustness of patient 8. Positive-step Time-to-Target indices for each controller. (1) Blue box: PID controller. (2) Green box: FOPID IAE. (3) Yellow box: FOPID ISO1. (4) Red box: FOPID ISO2. Outliers are marked with red crosses.

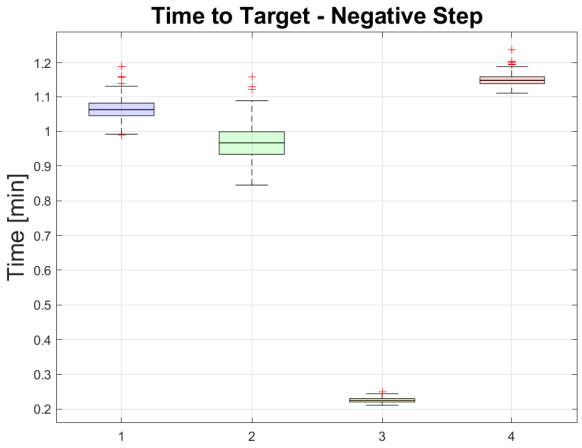

Figure 47. Intra-patient robustness of patient 8. Negative-step Time-to-Target indices for each controller. (1) Blue box: PID controller. (2) Green box: FOPID IAE. (3) Yellow box: FOPID ISO1. (4) Red box: FOPID ISO2. Outliers are marked with red crosses.

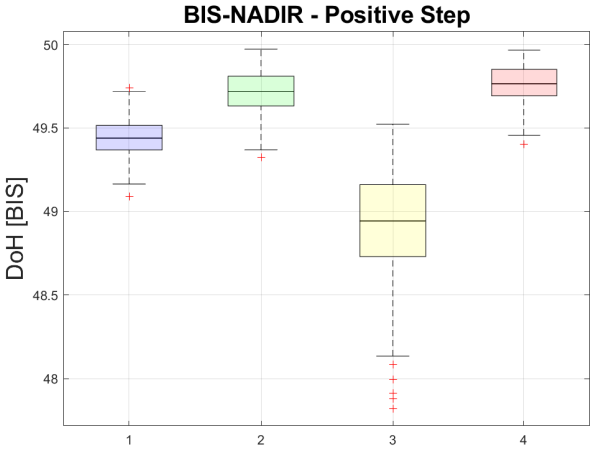

Figure 48. Intra-patient robustness of patient 8. Positive-step BIS-NADIR indices for each controller. (1) Blue box: PID controller. (2) Green box: FOPID IAE. (3) Yellow box: FOPID ISO1. (4) Red box: FOPID ISO2. Outliers are marked with red crosses.

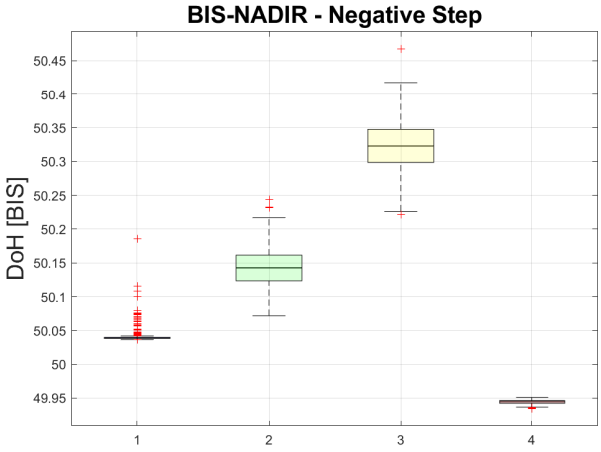

Figure 49. Intra-patient robustness of patient 8. Negative-step BIS-NADIR indices for each controller. (1) Blue box: PID controller. (2) Green box: FOPID IAE. (3) Yellow box: FOPID ISO1. (4) Red box: FOPID ISO2. Outliers are marked with red crosses.

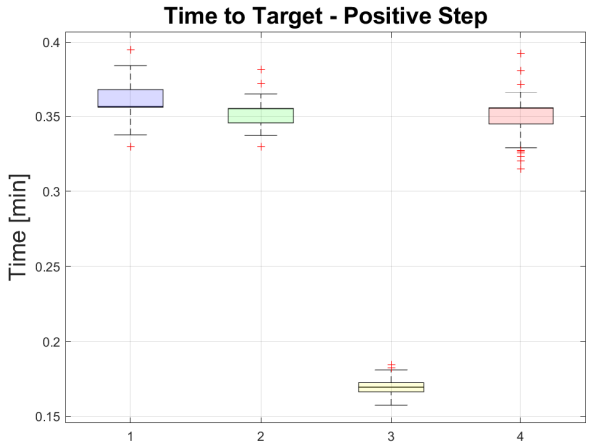

Figure 50. Intra-patient robustness of patient 9. Positive-step Time-to-Target indices for each controller. (1) Blue box: PID controller. (2) Green box: FOPID IAE. (3) Yellow box: FOPID ISO1. (4) Red box: FOPID ISO2. Outliers are marked with red crosses.

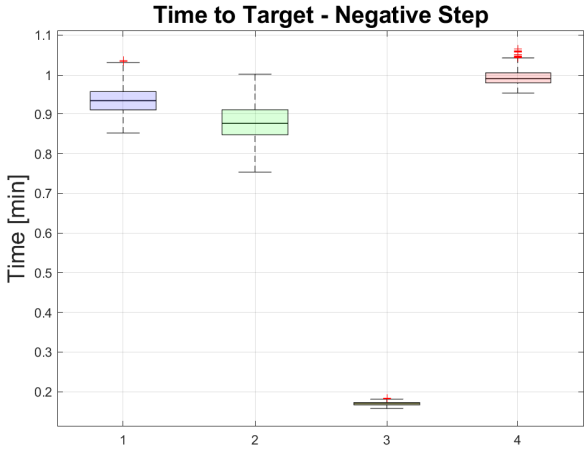

Figure 51. Intra-patient robustness of patient 9. Negative-step Time-to-Target indices for each controller. (1) Blue box: PID controller. (2) Green box: FOPID IAE. (3) Yellow box: FOPID ISO1. (4) Red box: FOPID ISO2. Outliers are marked with red crosses.

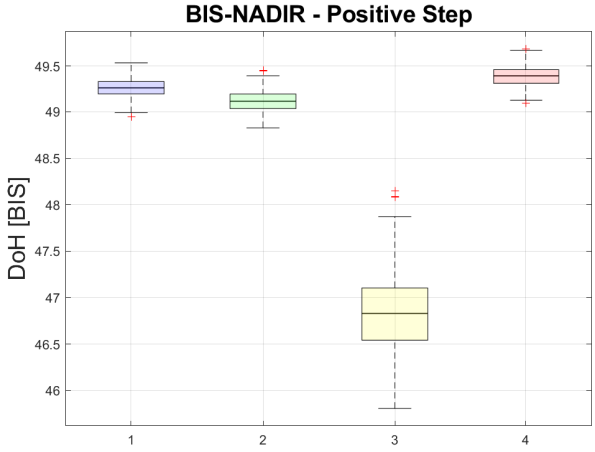

Figure 52. Intra-patient robustness of patient 9. Positive-step BIS-NADIR indices for each controller. (1) Blue box: PID controller. (2) Green box: FOPID IAE. (3) Yellow box: FOPID ISO1. (4) Red box: FOPID ISO2. Outliers are marked with red crosses.

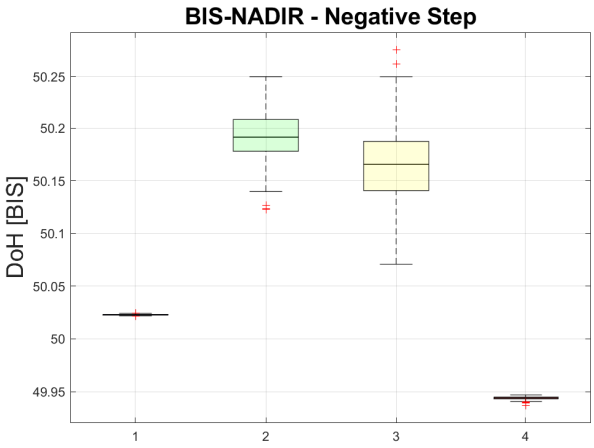

Figure 53. Intra-patient robustness of patient 9. Negative-step BIS-NADIR indices for each controller. (1) Blue box: PID controller. (2) Green box: FOPID IAE. (3) Yellow box: FOPID ISO1. (4) Red box: FOPID ISO2. Outliers are marked with red crosses.

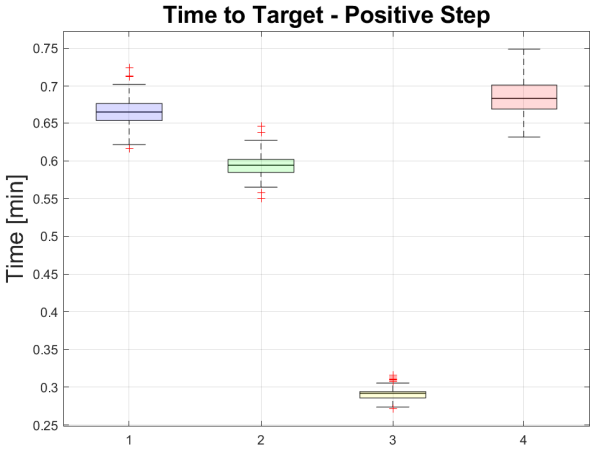

Figure 54. Intra-patient robustness of patient 10. Positive-step Time-to-Target indices for each controller. (1) Blue box: PID controller. (2) Green box: FOPID IAE. (3) Yellow box: FOPID ISO1. (4) Red box: FOPID ISO2. Outliers are marked with red crosses.

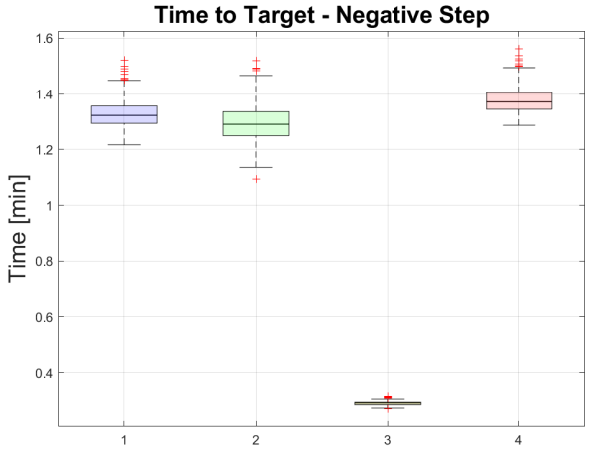

Figure 55. Intra-patient robustness of patient 10. Negative-step Time-to-Target indices for each controller. (1) Blue box: PID controller. (2) Green box: FOPID IAE. (3) Yellow box: FOPID ISO1. (4) Red box: FOPID ISO2. Outliers are marked with red crosses.

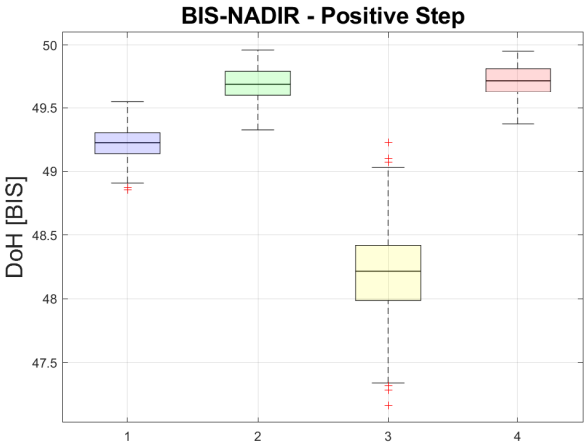

Figure 56. Intra-patient robustness of patient 10. Positive-step BIS-NADIR indices for each controller. (1) Blue box: PID controller. (2) Green box: FOPID IAE. (3) Yellow box: FOPID ISO1. (4) Red box: FOPID ISO2. Outliers are marked with red crosses.

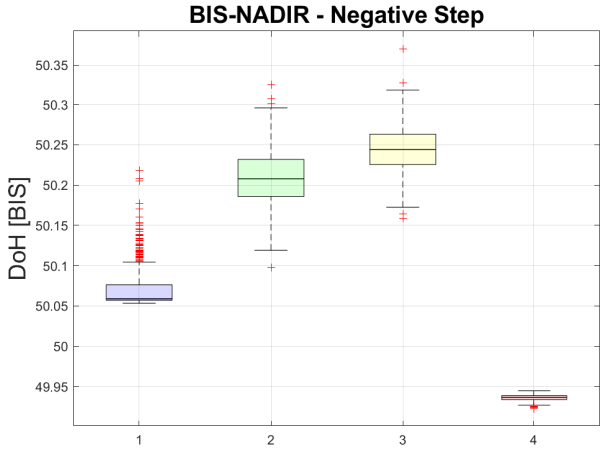

Figure 57. Intra-patient robustness of patient 10. Negative-step BIS-NADIR indices for each controller. (1) Blue box: PID controller. (2) Green box: FOPID IAE. (3) Yellow box: FOPID ISO1. (4) Red box: FOPID ISO2. Outliers are marked with red crosses.

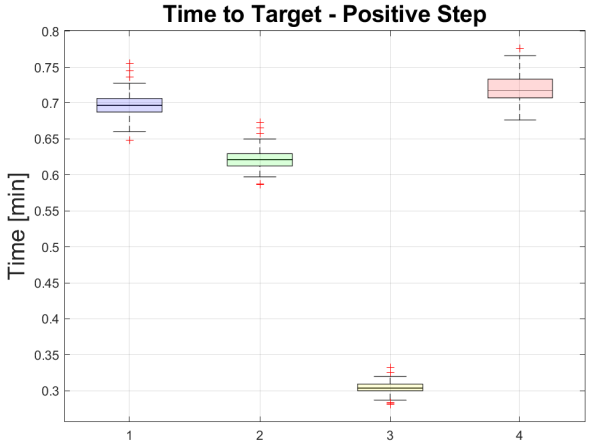

Figure 58. Intra-patient robustness of patient 11. Positive-step Time-to-Target indices for each controller. (1) Blue box: PID controller. (2) Green box: FOPID IAE. (3) Yellow box: FOPID ISO1. (4) Red box: FOPID ISO2. Outliers are marked with red crosses.

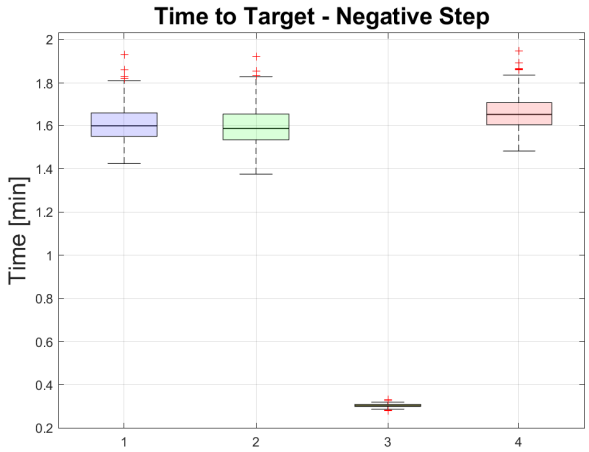

Figure 59. Intra-patient robustness of patient 11. Negative-step Time-to-Target indices for each controller. (1) Blue box: PID controller. (2) Green box: FOPID IAE. (3) Yellow box: FOPID ISO1. (4) Red box: FOPID ISO2. Outliers are marked with red crosses.

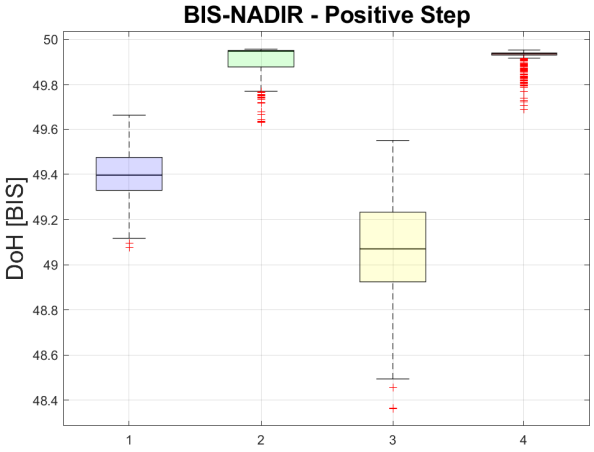

Figure 60. Intra-patient robustness of patient 11. Positive-step BIS-NADIR indices for each controller. (1) Blue box: PID controller. (2) Green box: FOPID IAE. (3) Yellow box: FOPID ISO1. (4) Red box: FOPID ISO2. Outliers are marked with red crosses.

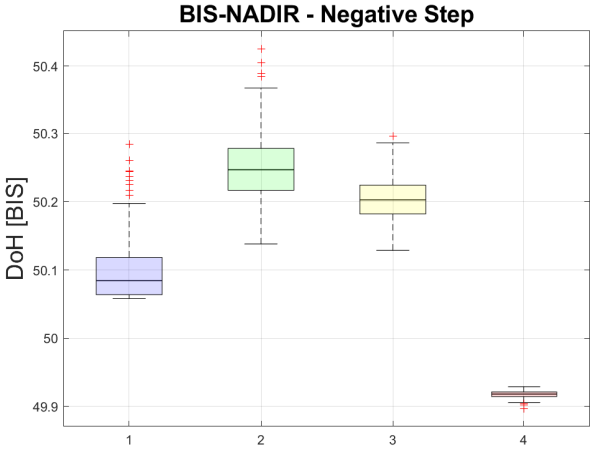

Figure 61. Intra-patient robustness of patient 11. Negative-step BIS-NADIR indices for each controller. (1) Blue box: PID controller. (2) Green box: FOPID IAE. (3) Yellow box: FOPID ISO1. (4) Red box: FOPID ISO2. Outliers are marked with red crosses.

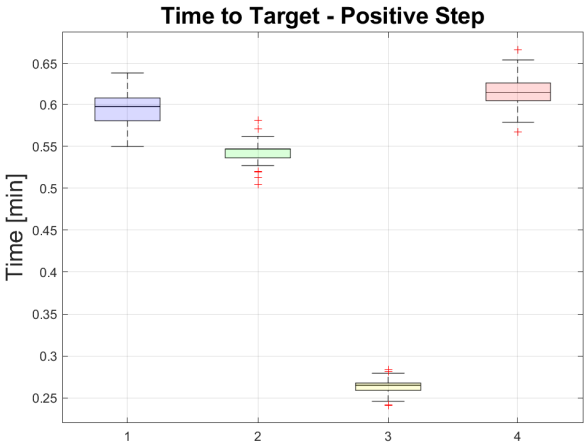

Figure 62. Intra-patient robustness of patient 12. Positive-step Time-to-Target indices for each controller. (1) Blue box: PID controller. (2) Green box: FOPID IAE. (3) Yellow box: FOPID ISO1. (4) Red box: FOPID ISO2. Outliers are marked with red crosses.

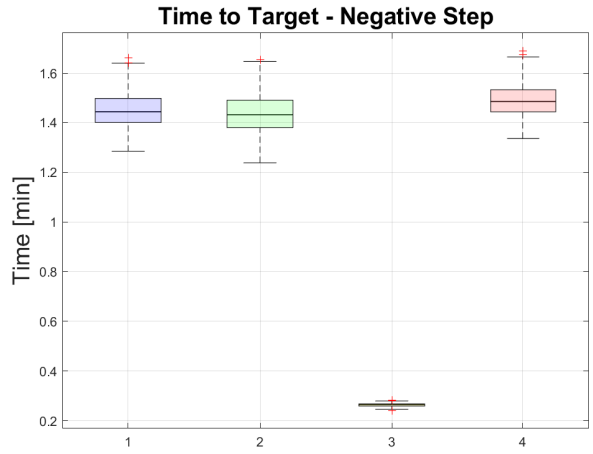

Figure 63. Intra-patient robustness of patient 12. Negative-step Time-to-Target indices for each controller. (1) Blue box: PID controller. (2) Green box: FOPID IAE. (3) Yellow box: FOPID ISO1. (4) Red box: FOPID ISO2. Outliers are marked with red crosses.

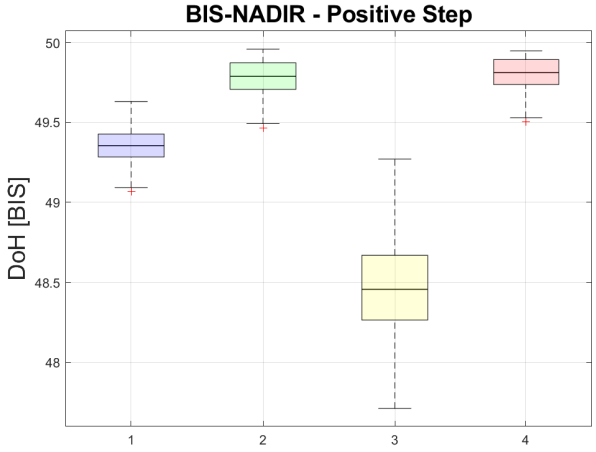

Figure 64. Intra-patient robustness of patient 12. Positive-step BIS-NADIR indices for each controller. (1) Blue box: PID controller. (2) Green box: FOPID IAE. (3) Yellow box: FOPID ISO1. (4) Red box: FOPID ISO2. Outliers are marked with red crosses.

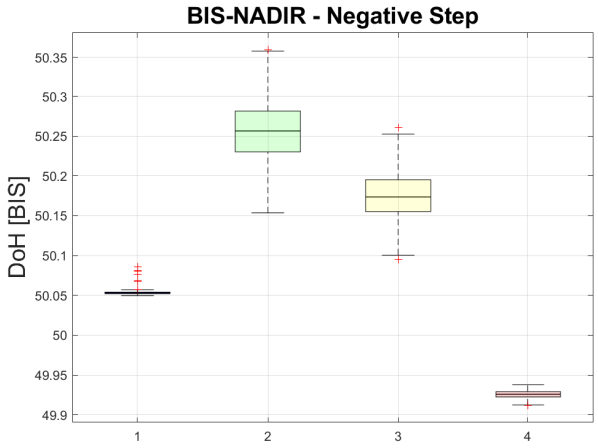

Figure 65. Intra-patient robustness of patient 12. Negative-step BIS-NADIR indices for each controller. (1) Blue box: PID controller. (2) Green box: FOPID IAE. (3) Yellow box: FOPID ISO1. (4) Red box: FOPID ISO2. Outliers are marked with red crosses.

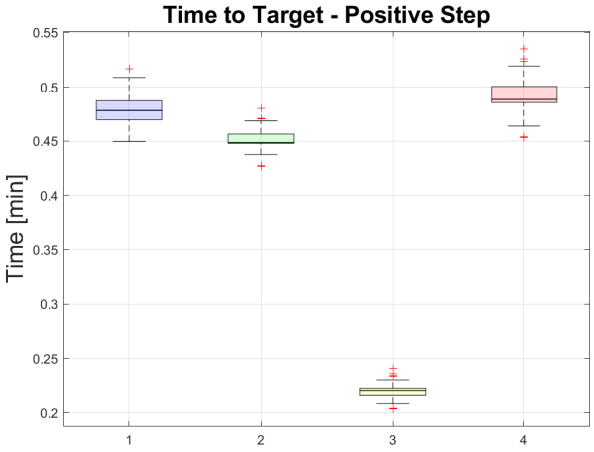

Figure 66. Intra-patient robustness of patient 13. Positive-step Time-to-Target indices for each controller. (1) Blue box: PID controller. (2) Green box: FOPID IAE. (3) Yellow box: FOPID ISO1. (4) Red box: FOPID ISO2. Outliers are marked with red crosses.

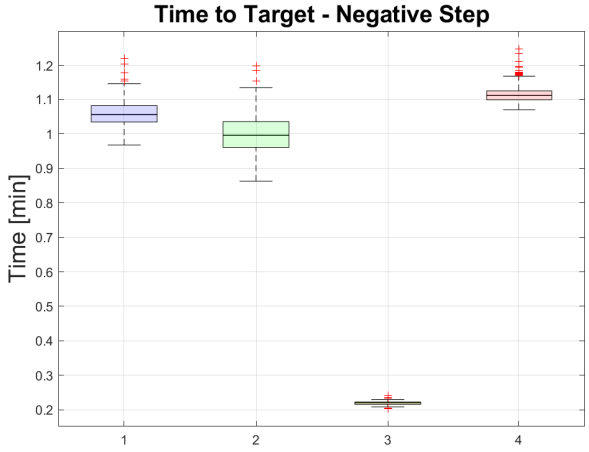

Figure 67. Intra-patient robustness of patient 13. Negative-step Time-to-Target indices for each controller. (1) Blue box: PID controller. (2) Green box: FOPID IAE. (3) Yellow box: FOPID ISO1. (4) Red box: FOPID ISO2. Outliers are marked with red crosses.

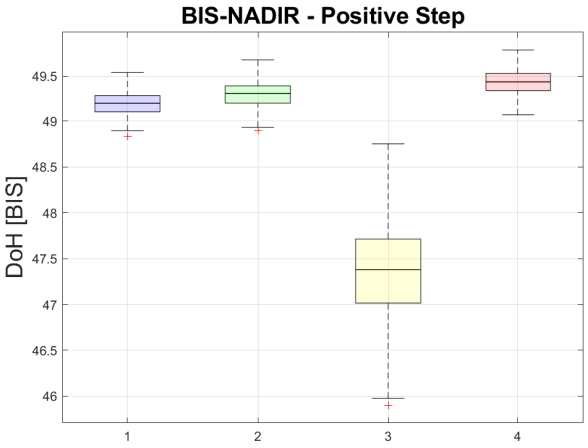

Figure 68. Intra-patient robustness of patient 13. Positive-step BIS-NADIR indices for each controller. (1) Blue box: PID controller. (2) Green box: FOPID IAE. (3) Yellow box: FOPID ISO1. (4) Red box: FOPID ISO2. Outliers are marked with red crosses.

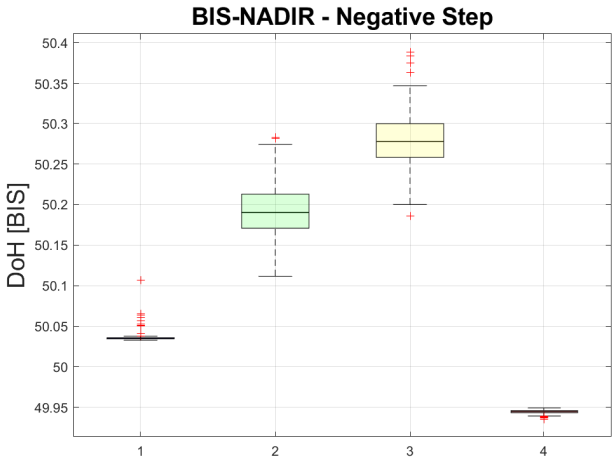

Figure 69. Intra-patient robustness of patient 13. Negative-step BIS-NADIR indices for each controller. (1) Blue box: PID controller. (2) Green box: FOPID IAE. (3) Yellow box: FOPID ISO1. (4) Red box: FOPID ISO2. Outliers are marked with red crosses.

4. Discussion

The results presented in Section 3 show that, with a fractional-order PID controller, it is possible to achieve a satisfactory performance (all the clinical requirements are met) in the maintenance phase of anesthesia during surgical procedures. From the presented results, it appears that tuning a FOPID controller by minimizing the IAE provides a slightly better performance compared to that obtained when the isodamping condition is imposed. All the analyzed controllers are able to handle both inter- and intra-patient variabilities, providing adequate robustness. From the performed simulations, it appears in any case that the performance obtained with a FOPID controller is very similar to that obtained with a PID controller. Therefore, it can be concluded that a FOPID closed-loop control system can be used to titrate propofol to achieve the required Depth of Hypnosis, but a traditional PID controller seems to still be the best option in terms of the trade-off between performance and the complexity of implementation. Given the encouraging results obtained from this simulation study, it would be interesting to test the FOPID-based control structure in a real clinical scenario. Since the Oustaloup approximation [29] was exploited during the design phase of the fractional-order controller, the controller transfer function turns out to be of high order. Anyway, it is still possible to perform controller discretization in order to implement it in control software that was used for clinical investigation [8,32]. Moreover, since the proposed control solution does not take into account the analgesic drug infusion, this variable will be manually regulated by the anesthesiologist, and it will be seen as a disturbance from the controller. In future works, a fractional-order PID controller will be designed for both components of anesthesia (i.e., hypnosis and analgesia) by exploiting a MISO system that considers both the propofol and remifentanil flow rates as control actions and the BIS as the only process variable.

5. Conclusions

In this paper, a thorough comparison between PID and FOPID controllers for DoH control through propofol administration during general anesthesia is presented. Two different tuning methods were applied to FOPID controllers, namely, the minimization of the IAE and the minimization of the maximum sensitivity by applying an isodamping approach (which cannot be used with PID controllers). From the presented simulation results, it appears that a FOPID is an effective solution, as it allows the clinical requirements to be met in terms of performance and robustness. However, the FOPID controller does not significantly improve on the performance achieved with the PID controller tuned by minimizing the IAE.

Author Contributions: Conceptualization, N.P., M.S., F.P. and A.V.; Methodology, N.P., F.P. and A.V.; Software, N.P.; Validation, M.S., N.L. and M.P.; Resources, N.L.; Writing—original draft, N.P.; Writing—review & editing, M.S., F.P. and A.V.; Supervision, N.L., M.P. and A.V. All authors have read and agreed to the published version of the manuscript.

Funding: This work was partially supported by the European Union NextGeneration EU (PIANO NAZIONALE DI RIPRESA E RESILIENZA (PNRR)—MISSIONE 4 COMPONENTE 2, INVESTIMENTO 3.3—Decreto del Ministero dell'Università e della Ricerca n.352 del 09/04/2022).

Institutional Review Board Statement: Not applicable.

Informed Consent Statement: Not applicable.

Data Availability Statement: Data sharing not applicable.

Conflicts of Interest: The authors declare no conflict of interest.

References

1. Copot, D.; Ionescu, C.M. Drug delivery system for general anesthesia: Where are we? In Proceedings of the IEEE International Conference on Systems, Man, and Cybernetics (SMC), San Diego, CA, USA, 5–8 October 2014; pp. 2452–2457.
2. Ghita, M.; Neckebroek, M.; Muresan, C.; Copot, D. Closed-Loop Control of Anesthesia: Survey on Actual Trends, Challenges and Perspectives. *IEEE Access* **2020**, *8*, 206264–206279. [CrossRef]
3. Padula, F.; Ionescu, C.; Latronico, N.; Paltenghi, M.; Visioli, A.; Vivacqua, G. Optimized PID control of depth of hypnosis in anesthesia. *Comput. Methods Programs Biomed.* **2017**, *144*, 21–35. [CrossRef] [PubMed]
4. Liu, N.; Chazot, T.; Genty, A.; Landais, A.; Restoux, A.; McGee, K.; Laloë, P.; Trillat, B.; Barvais, L.; Fischler, M. Titration of propofol for anesthetic induction and maintenance guided by the bispectral index: Closed-loop versus manual control: A prospective, randomized, multicenter study. *Anesthesiology* **2006**, *104*, 686–695. [CrossRef] [PubMed]
5. Puri, G.D.; Kumar, B.; Aveek, J. Closed-loop anaesthesia delivery system (CLADS™) using bispectral index: A performance assessment study. *Anaesth. Intensive Care* **2007**, *35*, 357–362. [CrossRef] [PubMed]
6. Soltesz, K.; Hahn, J.; Hägglund, T.; Dumont, G.A.; Ansermino, J.M. Individualized closed-loop control of propofol anesthesia: A preliminary study. *Biomed. Signal Process. Control* **2013**, *8*, 500–508. [CrossRef]
7. Schiavo, M.; Padula, F.; Latronico, N.; Paltenghi, M.; Visioli, A. Individualized PID Tuning for maintenance of general anesthesia with propofol. *IFAC-PapersOnLine* **2021**, *54*, 679–684. [CrossRef]
8. Schiavo, M.; Padula, F.; Latronico, N.; Paltenghi, M.; Visioli, A. A modified PID-based control scheme for Depth-of-Hypnosis control: Design and experimental results. *Comput. Methods Programs Biomed.* **2022**, *219*, 106763. [CrossRef]
9. Merigo, L.; Beschi, M.; Padula, F.; Latronico, N.; Paltenghi, M.; Visioli, A. Event-based control of depth of hypnosis in anesthesia. *Comput. Methods Programs Biomed.* **2017**, *147*, 63–83. [CrossRef]
10. Dumont, G.A.; Martinez, A.; Ansermino, J.M. Robust control of depth of anesthesia. *Int. J. Adapt. Control Signal Process.* **2009**, *23*, 435–454. [CrossRef]
11. Patel, B.; Patel, H.; Shah, D.; Sarvaia, A. Control strategy with multivariable fault tolerance module for automatic intravenous anesthesia. *Biomed. Eng. Lett.* **2020**, *10*, 555–578. [CrossRef]
12. Alavi, M.B.; Tabatabaei, M. Control of depth of anaesthesia using fractional-order adaptive high-gain controller. *IET Syst. Biol.* **2019**, *13*, 36–42. [CrossRef]
13. Navarro-Guerrero, G.; Tang, Y. Fractional order model reference adaptive control for anesthesia. *Int. J. Adapt. Control Signal Process.* **2017**, *31*, 1350–1360. [CrossRef]
14. Navarro-Guerrero, G.; Tang, Y. Fractional-order closed-loop model reference adaptive control for anesthesia. *Algorithms* **2018**, *11*, 106. [CrossRef]
15. Copot, D.; Muresan, C.I.; Keyser, R.D.; Ionescu, C.M. Patient specific model based induction of hypnosis using fractional order control. *IFAC-PapersOnLine* **2017**, *50*, 15097–15102. [CrossRef]
16. Chen, Y.Q.; Moore, K.L. Relay feedback tuning of robust PID controllers with iso-damping property. *IEE Trans. Syst. Man, Cybern.-Part B* **2005**, *35*, 23–31. [CrossRef]
17. Hegedus, E.; Birs, I.; Muresan, C.I. Fractional Order Control of the Combined Anaesthesia-Hemodynamic System: A Preliminary Study. *IFAC-PapersOnLine* **2021**, *54*, 19–24. [CrossRef]
18. Hegedus, E.T.; Birs, I.R.; Ghita, M.; Muresan, C.I. Fractional-Order Control Strategy for Anesthesia–Hemodynamic Stabilization in Patients Undergoing Surgical Procedures. *Fractal Fract.* **2022**, *6*, 614. [CrossRef]
19. Sahoo, S.K.; Prasad, S.; Srivastava, V.; Chhabra, H.; Yadav, J. Design of FOPID Controller for Regulating Anesthesia. In *Soft Computing: Theories and Applications*; Pant, M., Sharma, T., Verma, O., Singla, R., Sikander, A. Eds.; Advances in Intelligent Systems and Computing; Springer: Singapore, 2020; Volume 1053.
20. Birs, I.; Copot, D.; Muresan, C.I.; Keyser, R.D.; Ionescu, C.M. Robust fractional order PI control for cardiac output stabilisation. *IFAC-PapersOnLine* **2019**, *52*, 994–999. [CrossRef]

21. Copot, D.; Muresan, C.I.; Birs, I.; Kovacs, L. Robust Hemodynamic Control Under General Anesthesia Conditions. *IFAC-PapersOnLine* **2020**, *53*, 16179–16184. [CrossRef]
22. Schiavo, M.; Padula, F.; Latronico, N.; Merigo, L.; Paltenghi, M.; Visioli, A. Performance Evaluation of an Optimized PID Controller for Propofol and Remifentanil Coadministration in General Anesthesia. *IFAC J. Syst. Control* **2021**, *15*, 100121. [CrossRef]
23. Beschi, M.; Padula, F.; Visioli, A. The generalized isodamping approach for robust fractional PID controllers design. *Int. J. Control* **2017**, *90*, 1157–1164. [CrossRef]
24. Schnider, T.W.; Minto, C.F.; Gambus, P.L.; Andresen, C.; Goodale, D.B.; Shafer, S.L.; Youngs, E.J. The influence of Method of Administration and Covariates on the Pharmacokinetics of Propofol in Adult Volunteers. *J. Am. Soc. Anesthesiol.* **1998**, *88*, 1170–1182. [CrossRef] [PubMed]
25. Schnider, T.W.; Minto, C.F.; Shafer, S.L.; Gambus, P.L.; Andresen, C.; Goodale, D.B.; Youngs, E.J. The influence of Age on Propofol Pharmacodynamics. *J. Am. Soc. Anesthesiol.* **1999**, *90*, 1502–1516. [CrossRef]
26. Visioli, A. *Practical PID Control*, 1st ed.; Springer: London, UK, 2006; pp. 35–60.
27. Ionescu, C.M.; Keyser, R.D.; Torrico, B.C.; Smet, T.D.; Struys, M.M.R.F.; Normey-Rico, J.E. Robust Predictive Control Strategy Applied for Propofol Dosing Using BIS as a Controlled Variable During Anesthesia. *IEEE Trans. Biomed. Eng.* **2008**, *55*, 2161–2170. [CrossRef]
28. Padula, F.; Visioli, A.; Pagnoni, M. On the anti-windup schemes for fractional-order PID controllers. In Proceedings of the IEEE 17th International Conference on Emerging Technologies & Factory Automation, Krakow, Poland, 17–21 September 2012; pp. 1–4.
29. Oustaloup, A.; Cois, O.; Lanusse, P.; Melchior, P.; Moreau, X.; Sabatier, J. The CRONE approach: Theoretical developments and major applications. In Proceedings of the 2nd IFAC Workshop on Fractional DIfferentiation and Its Applications, Luxembourg, 19–21 July 2006; pp. 324–354.
30. Vanluchene, A.L.G.; Vereecke, H.; Thas, O.; Mortier, E.P.; Shafer, S.L.; Struys, M.M.R.F. Spectral entropy as an electroencephalographic measure of anesthetic drug effect: A comparison with bispectral index and processed midlatency auditory evoked response. *J. Am. Soc. Anesthesiol.* **2004**, *101*, 34–42. [CrossRef]
31. Soltesz, K. *On Automation in Anesthesia*; Department of Automatic Control, Lund University: Lund, Sweden, 2013.
32. Schiavo, M.; Padula, F.; Latronico, N.; Paltenghi, M.; Visioli, A. Experimental results of an event-based PID control system for propofol and remifentanil coadministration. *Control Eng. Pract.* **2023**, *131*, 105384. [CrossRef]